Supernovae in the nuclear regions of starburst galaxies

S. Mattila* and W.P.S.Meikle

Astrophysics Group, Blackett Laboratory, Imperial College of Science, Technology and Medicine, Prince Consort Road,
London SW7 2BW

ABSTRACT
The feasibility of using near-infrared observations to discover supernovae in the nuclear and circumnuclear regions of nearby starburst galaxies is investigated. We provide updated estimates of the intrinsic core-collapse supernova rates in these regions. We discuss the problem of extinction, and present new estimates of the extinction towards 33 supernova remnants in the starburst galaxy M 82. This is done using H I and H_2 column density measurements. We estimate the molecular to atomic hydrogen mass ratio to be 7.4 ± 1.0 in M 82. We have assembled near-infrared photometric data for a total of 13 core-collapse supernovae, some unpublished hitherto. This constitutes the largest database of IR light curves for such events. We show that the IR light curves fall into two classes, "ordinary" and "slow-declining". Template $JHKL$ light curves are derived for both classes. For ordinary core-collapse supernovae, the average peak $JHKL$ absolute magnitudes are –18.4, –18.6, –18.6, and –19.0 respectively. The slow-declining core-collapse SNe are found to be significantly more luminous than the ordinary events, even at early times, having average peak $JHKL$ absolute magnitudes of –19.9, –20.0, –20.0, and –20.4 respectively. We investigate the efficiency of a computerised image subtraction method in supernova detection. We then carry out a Monte Carlo simulation of a supernova search using K-band images of NGC 5962. The effects of extinction and observing strategy are discussed. We conclude that a modest observational programme will be able to discover a number of nuclear supernovae.

Key words: supernovae – starburst galaxies – image subtraction.

1 INTRODUCTION

Core-collapse supernovae (SNe) are observed to occur in sites of recent star formation. Such regions contain large quantities of dust, especially the nuclear ($r \lesssim 500$ pc) regions of starburst galaxies. Consequently, SN search programmes working at optical wavelengths probably miss a significant number of events in starburst galaxies due to dust obscuration. Thus, the observed supernova rates may be only a lower limit for the true supernova rate. The inferred star formation rates and radio observations of young supernova remnants (SNRs) indicate that highly-extinguished supernovae should exist in the nuclear regions of nearby starburst galaxies. In NGC 253 (*e.g.* Ulvestad & Antonucci 1997), NGC 2146 (Tarchi *et al.* 2000), M 82 (*e.g.* Allen & Kronberg 1998) and NGC4038/39 (Neff & Ulvestad 2000), several compact nonthermal radio sources have been identified as young SNRs indicating explosion rates of obscured supernovae of around 0.1 yr^{-1}. Also, high resolution radio observations have recently revealed a group of luminous radio supernovae in the

nuclear regions of ARP 220 (Smith *et al.* 1998). Yet only one supernova event (SN 1940E in NGC 253) has ever been directly observed in (or in front of) the nuclear regions in any of these five galaxies.

It is desirable to discover and study SNe in the centres of nearby starburst galaxies. In addition to providing a better estimate of the core-collapse rate in the local universe, such a survey would offer an opportunity to study the behaviour of supernovae in the dusty and dense nuclear environment and to probe the nuclear extinction. Indeed, SNe exploding in the nuclear regions of galaxies may differ significantly from ordinary SNe due to the higher density environment as suggested in the starburst model for AGN (Terlevich *et al.* 1992). The best-studied example of a core-collapse SN exploding within a high density circumstellar environment is SN 1998S (Fassia *et al.* 2000a, Fassia *et al.* 2000b, Gerardy *et al.* 2000, Leonard *et al.* 2000). Ultimately, such a survey would also be valuable in guiding attempts to determine the rates of high redshift core-collapse supernovae. Such a high redshift study is one of the aims of the NGST (New Generation Space Telescope) (Jorgensen *et al.* 1997; Madau *et al.* 1998, Dahlen & Fransson 1999; Sullivan *et al.*

* Send offprint requests to: s.mattila@ic.ac.uk

2000). However, before starting to investigate the evolution of the SN rate with redshift it is important to have an accurate measurement of the local SN rate and to understand the behaviour of supernovae within the dusty, high density starburst regions of galaxies.

The feasibility of searching for obscured supernovae in nuclear starburst regions has been discussed in two papers. Van Buren & Norman (1989) considered the use of mid-IR narrow-band (10.52 μm) imaging. They estimated that supernovae would be observable in the mid-IR with ground-based 4-10 m telescopes at distances of 15-40 Mpc in one night's integration. Supernova detection in the K-band was studied by Grossan *et al.* (1999). They emphasised the need for high spatial resolution to allow successful image subtraction in the nuclear regions of galaxies.

An optical search for supernovae in a sample of 142 nearby star-forming galaxies was carried out in 1988-1991 by Richmond *et al.* (1998). The observations were carried out with a 500×500 pixel CCD camera (0.58"/pixel) on a 1 m telescope at the Lick Observatory. Two search procedures were used. In the first method, the search images were compared by eye. This yielded five supernovae, all of which were outside the host galaxies' extinguished nuclear regions. The deduced SN rates were similar to those measured in normal galaxies. In the second method, differential photometry was carried out on the nuclei of the galaxies. However, they did not discover any brightening attributable to nuclear supernovae. From this, they deduced upper limits for the *unobscured* SN rates within the nuclear regions *viz.* $< 9h^2$ SRU[†], $< 12h^2$ SRU, and $< 7h^2$ SRU for Types Ia, Ib/c, and II, respectively. This work confirmed that, given the likely high obscuration in nuclear starbursts, for a search for supernovae in such regions to be successful it would have to be carried out at infrared wavelengths.

Van Buren *et al.* (1994) conducted a K-band survey for supernovae in starburst galaxies at NASA's Infrared Telescope Facility, Hawaii for about 2 years. Most of the observations were made with PROTOCam, and the Richardson-Lucy image restoration algorithm was used to enhance the resolution of the survey images. They discovered SN 1992bu in NGC 3690 in K-band images[‡]. The supernova is located $\sim$6" from Core B1 of the galaxy. They measured K-band magnitudes of +16.6, +17.2, and +18.1 in three images separated by about a month. No other observation of this supernova was reported, and thus it is not possible to say if it was located within the obscured nuclear regions.

A more recent (1992-1994) near-infrared (NIR) search for supernovae in 177 nearby IRAS galaxies has been carried out in the K'-band by Grossan *et al.* (1999). The observations were performed with the 2.3 m Wyoming IR Observatory (WIRO) telescope using the Michigan IR camera (MIRC), with a 2.2"/pixel resolution and 128×128 pixels. The seeing was typically between 0.7" and 1.0" and so the seeing disk was usually undersampled. The length of the time between two observations of a given galaxy varied typically from 1 to 3 months. They did not discover any su-

pernovae during the period, limiting the SN rate *outside the nuclear regions* (> 15" radius) to less than 3.8 FIRSRU[§] in their sample galaxies within 25 Mpc distance. They concluded that this negative result was due to the poor resolution of the camera and that a higher resolution NIR supernova search covering only the inner $\sim$450pc of each galaxy would be more productive.

The latest reported attempt to detect SN explosions in the nuclear regions of starburst galaxies was by Bregman *et al.* (2000). They observed a sample of 10 galaxies within 7 Mpc distance using ISOCAM with a pixel size of 3". After continuum subtraction they looked for traces of [Ni II] 6.63 μm line emission which would have indicated recent SN explosions. However, they did not detect any [Ni II] emission in the sample galaxies. They presented an upper limit for the SN rate in their galaxy sample normalised to M 82 viz. 0.3 yr^{-1}. Given the far-IR luminosity of M 82 (Appendix A) this corresponds to 7.2 FIRSRU.

Although, as argued above, the discovery of such SN events would clearly be important, given the uncertainties in *e.g.* nuclear extinction or SN magnitudes it is less obvious what might be achieved in practice with existing telescopes. We have therefore carried out a study to test the feasibility of discovering obscured supernovae in the nuclear regions of starburst galaxies. In this paper we report the results of this study. In Section 2, we review indirect methods of assessing the nuclear supernova rate and provide an updated estimate of this parameter. In Section 3, extinction towards nuclear supernovae is discussed. In particular, we present a new estimate of the extinction and its distribution in the starburst galaxy M 82. In Section 4, we present $JHKL$-band light curves for a total of 13 events, some unpublished hitherto. This constitutes the most complete database of core-collapse SN IR light curves ever published. We show that the IR light curves fall into two classes, "ordinary" and "slow-declining". Template $JHKL$ light curves are derived for both classes. In section 5, supernova detection using an image subtraction method is described and tested, and in section 6 Monte Carlo simulations are used to test the feasibility of a practical supernova search. The results are summarised in Section 7.

2   INDIRECT ESTIMATION OF THE NUCLEAR SUPERNOVA RATES

A wide variety of indirect methods have been employed to estimate the nuclear SN rates for nearby starburst galaxies. These include (a) observations of young SNRs using radio interferometry, (b) measurement of NIR [Fe II] luminosities of nuclear regions, and (c) measurement of non-thermal radio luminosities of nuclear regions. A collection of SN rate estimates from the literature is given in Table 1 for M 82, NGC 253, and NGC 4038/39.

Before examining these rate estimates, we note that the SN rates derived from optical search programmes are often given in terms of the SRU which has units of number of supernovae per century per $10^{10}L_\odot$ galaxy blue luminosity

---

[†] One SRU is the number of supernovae per century per $10^{10}L_\odot$ galaxy blue luminosity, and $H_0 = h \times 100$ kms^{-1}/Mpc.
[‡]
www.ipac.caltech.edu/ipac/info/sn1992/sn1992_NGC3690.html

[§] One FIRSRU is the number of supernovae per century per $10^{10}L_\odot$ galaxy far-IR luminosity (see Section 2).

Table 1. Indirect estimates of starburst nuclear supernova rates

Galaxy	r_{SN} (yr^{-1})	Method	Author
M82	>0.016	SNR source counts, radio source ages	Allen & Kronberg (1998)
M82	0.10	SNR source counts, radio source ages	Van Buren & Greenhouse (1994)
M82	0.05	SNR number vs. diameter relation	Muxlow *et al.* (1994)
M82	0.11±0.05	SNR number vs. diameter relation	Huang *et al.* (1994)
M82	<0.10	SNR source counts, lack of variability	Ulvestad & Antonucci (1994)
M82	∼0.1	[FeII] luminosity	Greenhouse *et al.* (1997)
M82	0.2	non-thermal radio luminosity	Colina & Perez-Olea (1992)
N253	0.08	SNR source counts, radio source ages	Van Buren & Greenhouse (1994)
N253	<0.30[a]	SN source counts, lack of variability	Ulvestad & Antonucci (1997)
N253	<0.10[b]	SN source counts, lack of variability	Ulvestad (2000)
N253	0.03	[FeII] luminosity	Engelbracht *et al.* (1998)
N253	0.05	non-thermal radio luminosity	Colina & Perez-Olea (1992)
N4038/39	∼0.2	compact non-thermal radio sources	Neff & Ulvestad (2000)

[a] for the innermost 200pc radius
[b] for the circumnuclear regions with radius between 200pc and 2kpc

(e.g. Cappellaro *et al.* (1999)). However, for nuclear starburst regions the high extinction means that definition of the SN rate in terms of the observed galaxy blue luminosity is rather pointless, since we cannot measure the intrinsic blue luminosity in the region of SN occurrence. Most of the optical-UV energy emitted by the massive stars is absorbed and re-radiated by dust in the FIR. We therefore express the SN rates in terms of the galaxy FIR luminosity (*i.e.* we use FIRSRU).

We can compare directly the estimated supernova rate with L_{FIR}. From Table 1, for M 82, NGC 253, and NGC 4038 we adopt SN rates of 0.1 yr^{-1}, 0.05 yr^{-1}, and 0.2 yr^{-1} respectively as representative of the range of estimates. If we then compare these values with the galaxies' L_{FIR} values (see Appendix A), we obtain a relation between the supernova rate and FIR luminosity:

$$r_{\mathrm{SN}} = 2.7 \times 10^{-12} \times L_{\mathrm{FIR}}/L_{\odot} \quad yr^{-1} \qquad (1)$$

The origin of this relation is now discussed. The core-collapse SN rate can be derived from the SFR [M$_{\odot}$yr^{-1}] (e.g. Madau *et al.* 1998) using :

$$r_{SN} = \frac{\int_{m_l}^{m_u} \phi(m)dm}{\int_{m_{min}}^{m_{max}} m\phi(m)dm} \times SFR \qquad (2)$$

where $\phi(m)$ is the IMF with lower and upper mass cut-offs of m_{min} and m_{max}, and where m_l and m_u are the lower and upper mass limits for a core-collapse SN progenitor. For SN progenitor masses between 8 and 50 M$_{\odot}$ (Tsujimoto *et al.* 1997) and a Salpeter IMF (m$^{-2.35}$) with cut-offs of 0.1 and 125 M$_{\odot}$ (*i.e.* stars of all possible masses are being formed) we obtain :

$$r_{\mathrm{SN}} = 0.0070 \times SFR \quad yr^{-1} \qquad (3)$$

Thus, if we can estimate the SFR in a starburst galaxy, we shall have an additional method for assessing the supernova rate. The SFRs can be estimated for a sample of galaxies via integrated emission line or continuum luminosities. A popular method for estimating the SFR is via the far–IR luminosity, L_{FIR}, of the galaxy. This requires us to

assume that the L_{FIR} is powered by a population of young, massive stars rather than by a population of old stars or an AGN. A number of authors have derived SFRs in this way, the estimates for the ratio SFR/L_{FIR} being in the range (1.5–6.5)×10^{-10} M$_{\odot}$yr^{-1}/L$_{\odot}$ (e.g. Thronson & Telesco 1986, Condon 1992, Buat & Xu 1996).

More recently Rowan-Robinson *et al.* (1997) indicated a relation between SFR and FIR luminosity using starburst models for optical-UV radiation assuming that a fraction ϵ of the optical-UV energy emitted in a starburst is absorbed and re-radiated by dust in the FIR. If stars of all possible masses are being formed according to the Salpeter IMF, we have :

$$SFR = \frac{1.5}{\epsilon} \times 10^{-10} L_{\mathrm{FIR}}/L_{\odot} \quad M_{\odot}yr^{-1} \qquad (4)$$

where $L_{\mathrm{FIR}} = L(8\text{-}1000\mu m)$[¶]. The choice of the IMF cut-offs is not critical here, as a change in the SFR resulting from a change in the cutoffs is mostly canceled when converting to the SN rate. This is because the stars exploding as core-collapse SNe are the same stars which produce the luminosity from which the SFR is estimated.

Applying this SFR estimate to equation (2) we obtain a relation between the supernova rate and starburst galaxy's FIR luminosity :

$$r_{\mathrm{SN}} = \frac{1.1}{\epsilon} \times 10^{-12} L_{\mathrm{FIR}}/L_{\odot} \quad yr^{-1} \qquad (5)$$

For starburst galaxies with high optical depths, ϵ is about 1. An example is Arp 220, whose $L_{\mathrm{FIR}} = 1.4 \times 10^{12} L_{\odot}$ would therefore imply a supernova rate of 1.5 per year. However, for galaxies like NGC 253, M 82, and NGC 4038 the value of ϵ is smaller (e.g. Silva *et al.* 1998). Given their L_{FIR} values of 4.2×10^{10}L$_{\odot}$, 1.9×10^{10}L$_{\odot}$, and 6.8×10^{10}L$_{\odot}$ respec-

[¶] The definition of FIR luminosity varies in literature. Throughout this paper we adopt $L_{\mathrm{FIR}}=L(8\text{-}1000\mu m)= 4\pi D_{\mathrm{L}}^2 \times 1.8\times 10^{-14}(13.48f_{12} + 5.16f_{25} + 2.58f_{60} + f_{100})$ [W] (Sanders and Mirabel 1996).

Table 2. Extinction estimates for the nuclei of starburst galaxies

Galaxy	A_V(center)	the method	the author
M82	2-12	NIR H lines (screen)	Satyapal *et al.* (1995)
M82	10	mid-IR line ratios (screen)	Genzel *et al.* (1998)
M82	1.19(K)	Brα/Brγ (screen)	Mouri *et al.* (1997)
M82	27	NIR & mm recomb. lines(screen)	Puxley *et al.* (1989)
NGC253	$\sim$9	NIR line ratios (screen)	Engelbracht*et al.* (1998)
NGC253	17-19	NIR colours (mixed)	Engelbracht *et al.* (1998)
NGC253	4-7	NIR colours (screen)	Engelbracht *et al.* (1998)
NGC253	35	NIR & mm recomb. lines(screen)	Puxley *et al.* (1997)
NGC253	30	mid-IR line ratios (mixed)	Genzel *et al.* (1998)
NGC3690A/B	20	mid-IR line ratios (mixed)	Genzel *et al.* (1998)
NGC4038/9	80	mid-IR line ratios (mixed)	Genzel *et al.* (1998)
NGC4194	0.57(K)	Brα/Brγ (screen)	Mouri *et al.* (1997)
NGC7469	20	mid-IR line ratios (mixed)	Genzel *et al.* (1998)
NGC7714	0.14(K)	Brα/Brγ (screen)	Mouri *et al.* (1997)
ARP220	45	mid-IR line ratios (screen)	Genzel *et al.* (1998)

tively, this implies SN rates exceeding 0.046, 0.021, and 0.075 per year, consistent with the typical values given in Table 1.

In summary, equ. (1) based on direct observations of SNRs is consistent with equ. (5) and agrees well with the r_{SN}–L_{FIR} relation obtained similarly by Van Buren & Greenhouse (1994). It is also similar to the *unobscured* type II+Ib/c SN rate of $(2.5 \pm 0.3) \times 10^{-12} \times L_{FIR} / L_\odot \; yr^{-1}$ obtained by Cappellaro *et al.* (1999). However, the typical ages of starbursts, 10–100Myr (e.g. Genzel *et al.* 1998), are comparable with the 5–50 Myr lifetimes of the core-collapse SN progenitors. Therefore, the relation between the SN rate and the galaxy's far–IR luminosity depends on the age of the burst (Fig. 13 in Genzel *et al.* 1998), rather than remaining the same from one starburst to another. Starburst models indicate ages of 20–30 Myrs for the bursts in M 82 (Efstathiou *et al.* 2000) and NGC 253 (Engelbracht *et al.* 1998). Thus, for a younger or much older starburst the SN rate would be somewhat smaller. Equ. 1 will be used later in this paper to estimate the SN rate for a sample of starburst galaxies.

3   EXTINCTION TOWARDS NUCLEAR SUPERNOVAE

The light from supernovae in starburst galaxies is scattered and absorbed by dust located both locally within the star formation regions in which the SNe occur, and at greater distances but still within their host galaxies. Near-IR recombination lines and colours are widely used for deriving the extinction towards starbursts because they suffer a lower extinction than optical lines. For example, Engelbracht *et al.* (1998) find $A_V = 4 - 19$ towards the nucleus of NGC 253. However, even near-IR lines may not probe deeply enough into these regions. Hydrogen ionisation rate studies of Puxley *et al.* (1997) based on NIR and mm-wavelength observations, and mid-IR line studies by Genzel *et al.* (1998) indicate considerably higher extinctions ($A_V = 30 - 35$) towards the NGC 253 nucleus. In Table 2 extinction estimates to galactic nuclei obtained by a range of techniques are listed for several galaxies. In estimating the extinction,

two extreme models are often considered *viz.* a foreground dust screen and a mixture of stars/gas and dust. These tend to respectively under- and over-estimate the extinction. $A_V(screen) \sim 10$ corresponds to $A_V(mixed) \geq 100$ (Genzel *et al.* 1998). It is also likely that the extinction is very patchy, adding further to the uncertainty in the true value. To reduce these uncertainties, we have carried out a new study of the extinction in M 82. This is now described.

3.1   Extinction towards the SNRs of M 82

An estimate of the extinction towards the SNRs in M 82 can be made if we know the total hydrogen (atomic + molecular) column densities to these objects. Wills *et al.* (1998) measured 21 cm atomic hydrogen absorption towards 33 individual SNRs in M 82 from which they derived H I column densities. Weiß *et al.* (2000) have used Large Velocity Gradient (LVG) calculations to obtain molecular hydrogen (H$_2$) column densities from high resolution ^{13}CO and C^{18}O observations for several lines-of-sight through M 82. By interpolation between these values they have provided estimates of the H$_2$ column densities through M 82 at the SNR positions (Weiß private communication). In Table 3 (upper section), col. 3 and 4 respectively, we give the column densities of atomic hydrogen towards the SNRs, N(H I)$_{SNR}$, and of molecular hydrogen through the whole galaxy along the line of sight (LOS) to the SNRs, N(H$_2$)$_{LOS}$. Using these values and assuming a conservative error of $\pm 50\%$ for the interpolated N(H$_2$) values, we obtain the ratio $2N$(H$_2$)$_{LOS}/N$(H I)$_{SNR}$ for each SNR. These are presented in Table 3, col. 5. We expect this ratio to have its smallest values for the SNRs which are located behind most of the molecular gas along the line of sight *i.e.* the minimum values give us an indication of the mass ratio of H$_2$ to H I along a given line-of-sight.

Uncertainties in the ratios are due to errors in the N(H I) values, the CO data entering the LVG calculations and the interpolations to the SNR positions. In order to make better use of the column density data, we follow the philosophy of the V/V$_{max}$ test (Schmidt 1968). In this we assume that $2N$(H$_2$)$_{LOS}/N$(H I)$_{LOS}$ has a single value for

Table 3. Extinction estimates for the SNRs of M 82. The right ascensions and declinations are offsets from 09h51m00s and +69d54m00s.

RA (1950.0) seconds	Dec (1950.0) arcsec	$N(\mathrm{H\,I})_{\mathrm{SNR}}$ $\times 10^{21}$ cm^{-2}	$N(\mathrm{H_2})_{\mathrm{LOS}}$ $\times 10^{21}$ cm^{-2}	$2N(\mathrm{H_2})_{\mathrm{LOS}}/$ $N(\mathrm{H\,I})_{\mathrm{SNR}}$	A_V
39.10	57.3	3.7 ± 0.6	110	59 ± 31	16 ± 3
39.40	56.1	>16	123	<15	>71
39.77	56.9	>6.5	113	<35	>29
40.62	56.0	9.3 ± 2	204	44 ± 24	41 ± 10
40.67	55.1	9.5 ± 0.2	160	34 ± 17	42 ± 5
41.30	59.6	4.7 ± 1	51	22 ± 12	21 ± 5
41.95	57.5	4.5 ± 0.1	26	12 ± 6	20 ± 2
42.53	61.9	7.7 ± 0.4	40	10 ± 5	34 ± 4
42.61	59.9	7.3 ± 0.8	46	13 ± 6	32 ± 5
42.65	61.5	7.0 ± 1	41	12 ± 6	31 ± 6
43.18	58.3	7.8 ± 0.3	41	11 ± 5	35 ± 4
43.22	61.2	9.5 ± 1	42	8.8 ± 5	42 ± 7
43.31	59.2	5.1 ± 0.1	41	16 ± 8	23 ± 3
43.74	62.5	5.3 ± 1	40	15 ± 8	24 ± 5
43.81	62.8	>13	39	<6	>58
44.01	59.6	4.8 ± 0.5	34	14 ± 7	21 ± 3
44.28	59.3	3.3 ± 0.5	35	21 ± 11	15 ± 3
44.51	58.2	6.0 ± 0.6	33	11 ± 6	27 ± 4
44.91	61.1	>9.0	55	<12	>40
45.17	61.2	19 ± 0.4	61	6.4 ± 3	85 ± 10
45.24	65.2	>22	110	<10	>98
45.48	64.8	>30	136	<9.1	>134
45.74	65.2	4.2 ± 2	105	50 ± 35	19 ± 9
45.89	63.8	>10	93	<19	>45
46.52	63.9	3.9 ± 2	54	28 ± 20	17 ± 9
46.70	67.1	6.0 ± 2	50	17 ± 10	27 ± 9
39.64	53.4	<6.8	-	-	<30
40.32	55.1	<9.5	-	-	<42
42.66	55.5	<2.5	-	-	<11
42.80	61.2	<2.7	-	-	<12
44.35	57.8	<3.3	-	-	<15
44.43	61.8	<2.2	-	-	<10
45.42	67.4	<1.6	-	-	<7

any line of sight through M 82. In addition, we assume that the SNRs are randomly distributed throughout M 82, and so we expect to have :

$$< \frac{N(H\ I)_{\mathrm{SNR}}}{N(H\ I)_{\mathrm{LOS}}} >= \frac{1}{2} \qquad (6)$$

Applying the test using the 19 sets of H I (excluding the upper and lower limits) and H$_2$ column densities (table 3), we find an H$_2$ to H I mass ratio of 7.4 ± 1.0. However, it should be noted that the H$_2$ column densities are model dependent introducing further uncertainty in the mass ratio. Nevertheless, our result is consistent with the lowest values listed in table 3, but has a higher precision. It is also in good agreement with the mass ratios of 7–10 suggested by Crutcher *et al.* (1978) and Yun *et al.* (1993) for the centre of M 82.

The extinction towards the M 82 SNRs was estimated adopting $A_V = 0.53 \times 10^{-21}$ $(N(H\ I) + 2N(H_2))$ cm^{-2} (Bohlin *et al.* 1978). This assumes that the dust properties and dust/gas ratio are the same for M 82 as for the Milky Way Galaxy. For each SNR, an estimate of A$_V$ was obtained by adopting 7.4 for the $2N(H_2)/N(H\ I)$ ratio and using the $N(H\ I)$ values. The extinctions are listed in Ta-

ble 3, col. 6. The uncertainties arise from errors in the $N(H\ I)$ measurements and in the adopted $2N(H_2)/N(H\ I)$ ratio. We note that the SNRs with the highest extinctions are located within the two CO lobes on the edges of the galaxy. It has been suggested that these lobes are associated with the ends of an edge-on ring structure or bar structure (Neiniger *et al.* 1998). Considering only those 19 SNRs for which we have $N(H\ I)$ values (as against lower or upper limits), we obtain a weighted mean extinction of A$_V = 24$ ($\sigma \sim 9$). However, M 82 is an almost edge-on galaxy and so, in general, the column densities will be considerably greater than for a face-on starburst galaxy. Incorporation of our M 82 extinction analysis into the feasibility study will be described in Section 6.1.

4 THE IR LIGHT CURVES OF CORE-COLLAPSE SUPERNOVAE

In order to investigate realistically the feasibility of discovering nuclear SN, we need to ascertain the IR luminosity and evolution of core-collapse SNe. To this end we have assembled near-IR photometric data for a total of 14 events, some of which has never been published. This constitutes the

Table 4. The supernova sample

SN	Type	t_{BVmax}[a]	Galaxy	distance (Mpc)	A_V[b]	M_J obs.	M_H obs.	M_K obs.	M_L obs.	M_J max	M_H max	M_K max	M_L max
1979C	IIL	43979	M 100	16.1(1.3)	0.71(0.1)	−19.67	−19.84	−19.95	−20.38	−19.9	−20.1	−20.2	−20.4
1980K	IIL	44543	NGC 6946	5.7(0.5)	1.1(0.2)	−18.69	−18.74	−18.83	−19.18	−18.7	−18.7	−18.8	−18.9
1983N	Ib	45533	NGC 5236	5.0(0.75)	0.85(0.5)	−18.31	−18.32	−18.40	−18.50	−18.3	−18.4	−18.4	−18.4
1990E	IIP	47960	NGC 1035	17.1(1.9)	1.5(0.3)	−18.02	−17.99	–	–	−18.0	−18.0	–	–
1993J	IIb	49095	M81	3.63(0.34)	0.58(0.4)	−17.95	−17.93	−18.06	–	−17.8	−17.9	−17.9	–
1994I	Ic	49451	M51	8.3(1.2)	1.4(0.3)	–	–	−17.19	–	–	–	−17.3	–
1998S	IIn	50890	NGC 3877	18.2(2.7)	0.68(0.1)	−19.47	−19.49	−19.48	–	−19.7	−19.6	−19.6	−20.4
[c] 1982E	Ib	45057	NGC 1332	19.0(2.9)	(0.8)	–	–	–	–	−16.7	−18.7	−19.9	–
1982R	Ib	45248	NGC 1187	17.5(2.6)	(0.8)	–	–	–	–	−17.6	−17.5	−17.7	−19.3
1983I	Ic	45443	NGC 4051	18.2(2.7)	(0.7)	–	–	–	–	−18.2	−18.7	−18.4	–
1984L	Ib	45943	NGC 991	20.1(3.0)	(0.8)	–	–	–	–	−19.0	−19.4	−19.1	–
1985L	IIL	46227	NGC 5033	20.0(3.0)	(0.7)	–	–	–	–	−20.3	−20.2	−20.1	−19.7
1985P	IIP	46349	NGC 1433	12.4(1.9)	(0.7)	–	–	–	–	−19.4	−19.4	−19.3	–

[a] Epoch in (Julian Days–2400000). Epoch references - 1979C: Panagia *et al.* (1980), 1980K: Dwek *et al.* (1983), 1982E: Maza (1982), 1982R: Muller & Pizarro (1982), 1983I: Elias *et al.* (1985), 1983N: Panagia *et al.* (2000), 1984L: Elias *et al.* (1985), 1985L: Kriss (1985), 1985P: Evans & Hazelbrook (1985), 1990E: Schmidt *et al.* (1993), 1993J: Lewis *et al.* (1994), 1994I: Iwamoto *et al.* (1994), 1998S: A. Fassia private communication.
[b] Extinction references - 1979C: Fesen *et al.* (1999), 1980K: Buta *et al.* (1982), 1983N: Panagia *et al.* (2000), 1990E: Schmidt *et al* (1993), 1993J: Richmond *et al.* (1994), 1994I: Iwamoto *et al.* (1994), 1998S: Fassia *et al.* (2000).
[c] The lower section lists SNe for which IR data are not available until at least 10 days after maximum BV light. For these events the peak magnitudes were estimated using the template light curve, and are quoted to a precision of only one figure after the decimal point. In addition, no extinction measurements are available for these SNe and so the extinctions were estimated assuming a host galaxy extinction of $A_V \sim 0.7$ plus the Galactic extinction according to Schlegel et al. (1998).

most complete database of core-collapse SN IR light curves to date. However, one event was SN 1987A, and although coverage of its IR light curves is unparalleled, they were highly atypical in luminosity and shape. We have therefore excluded this event. The photometric data for the remaining 13 SNe are listed in Appendix B. In Table 4 we list other information about these SNe. We have used these events to derive absolute magnitude "template" light curves to represent the typical core-collapse SN evolution in the IR.

Distances to the host galaxies are listed in Col. 5. For SN 1979C (Ferrarese *et al.* 1996) and SN 1993J (Freedman *et al.* 1994) these were obtained from HST Cepheid observations. For SN 1980K, Eastman *et al.* (1996), Buta *et al.* (1982), and Tully (1988) give similar distances using, respectively, the expanding photosphere method, photometric distance indicators, and recession velocities corrected for the expansion of the Local Super Cluster and the infall towards the Virgo Cluster. We adopted the average of these three values. For SN 1990E, we adopted the average of the similar distances given by Eastman *et al.* (1996), and Tully (1988). For the remaining nine SNe, we used the distances given by Tully (1988)[‖]. Estimates of the errors in the distances are given in parentheses.

For seven events (SNe 1979C, 80K, 83N, 90E, 93J, 94I, 98S) photometry is available for at least one of the $JHKL$ bands less than ∼10 days after maximum light in the BV-

band [⋆⋆]. Extinction estimates for these SNe are also available from the literature, and these are listed in Col. 6. These values were converted to A_J, A_H, A_K, and A_L assuming the galactic reddening law given by Rieke & Lebofsky (1985). Absolute intrinsic magnitudes near epoch 0 days were then determined by subtracting the distance moduli from the apparent magnitudes and correcting for extinction. These magnitudes are listed in Cols. 7-10. The other six events (SNe 1980E, 80R, 83I, 84L, 85L, 85P) were not observed until an epoch of later than 10 days. Moreover, no extinction estimates were available for these events. Therefore, the extinctions were estimated by adopting a typical host galaxy extinction of $A_V = 0.7$ and adding to this the appropriate Galactic extinction value given in Schlegel et al. (1998). The uncertainty in A_V is therefore quite large - we estimate ± 0.5. The peak magnitudes for these SNe given in Table 4 (cols. 11-14) are only estimates, obtained by extrapolating back to epoch +5 days for "ordinary" events and to ∼+10 days for "slowly-declining" events using the light curve templates described below.

Among the 13 events used to determine the absolute magnitude template light curves, we identify two classes of behaviour. In one class we have 4 supernovae (including types IIP, IIL, Ib) which decline linearly for at least

[‖] All the distances given by Tully (1988) have been scaled to H_0 = 70 kms^{-1} Mpc^{-1}.

[⋆⋆] The actual peak magnitude of core-collapse SNe is normally missed. "BV maximum light" in this context usually means the brightest observed magnitude on the already-declining light curve. However, in the case of SN 1983N, the B-band light curve was followed through the true maximum. In this paper we adopt the time of maximum light in the BV-band as epoch 0 days.
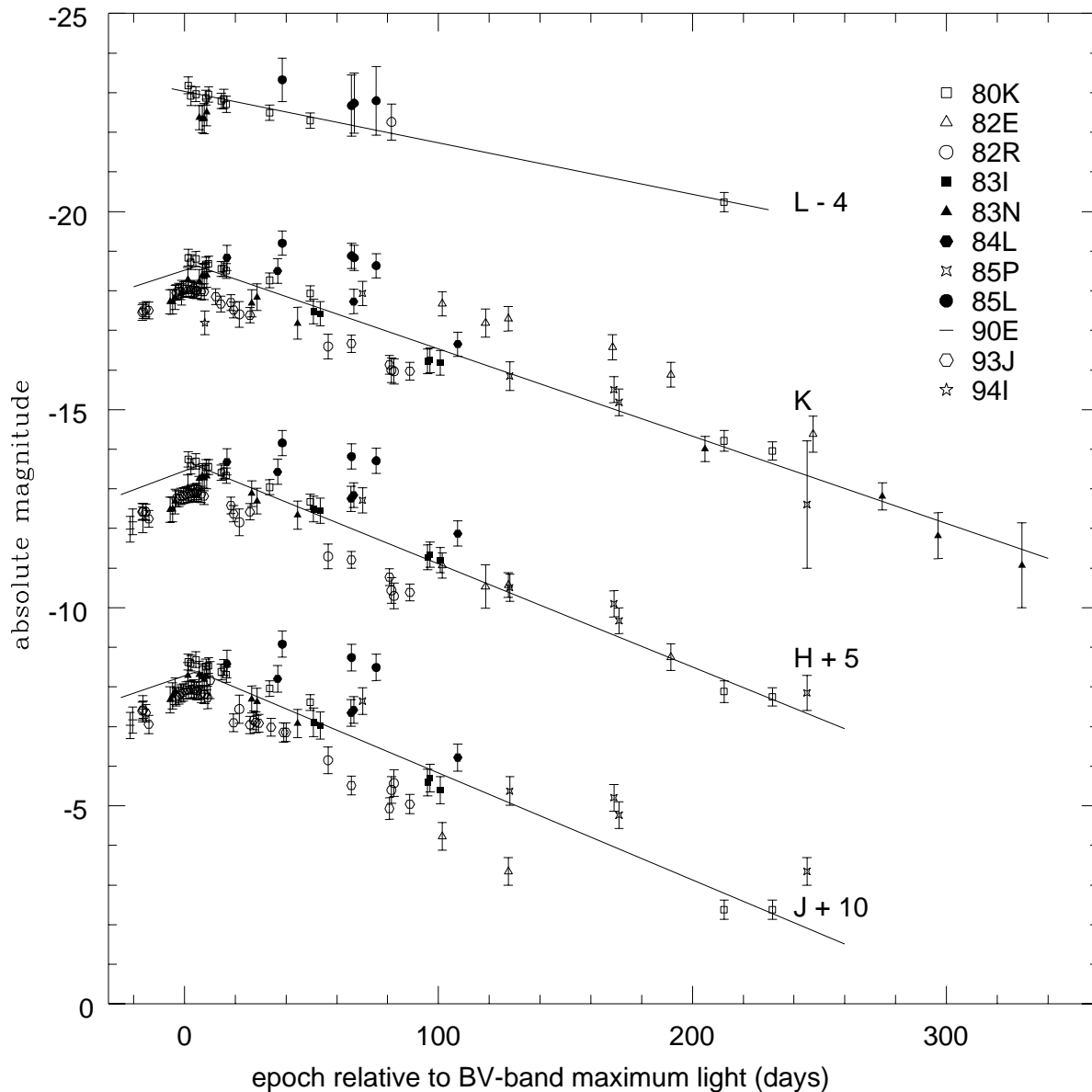
Figure 1. $JHKL$-band light curves and templates for "ordinary" core-collapse SNe. For clarity, the J, H, and L-band data and templates have been vertically displaced by +10, +5, and –4 magnitudes respectively. The horizontal positions of the individual light curves were set such that 0 days corresponds to BV-maximum (see text) in each case. The error bars give the combined uncertainties in photometry, extinction and distance.

~200 days after epoch 0 days. We shall refer to these as "ordinary" events. This class includes SNe 1980K, 82E, 83N and 85P. In the other class we have 2 "slowly-declining" supernovae, comprising the type IIL SN 1979C and the type IIn SN 1998S. From about 0 days to 100 days the JHK light curves of this class decline at a rate similar to that seen in the ordinary light curves. However, beyond ~100 days a much slower decline in J and H occurs, together with virtually no decline in K, persisting for over 450 days. Moreover, in the L band there is negligible decline from soon after the explosion to beyond 450 days. Recent observations show that the slowly-declining behaviour has persisted in SN 1998S for over 700 days. The remaining 7 events (SNe 1982R, 83I, 84L, 85L, 90E, 93J, 94I) all show a similar decline rate during the first 100 days to that seen in the ordinary and slowly-declining classes. They include types IIP, IIL, IIb and Ib/c. However, as they were not observed in the IR much beyond 100 days we are unable to distinguish which of the two classes, if either, they should be assigned to. We therefore, conservatively, assign them to the ordinary class.
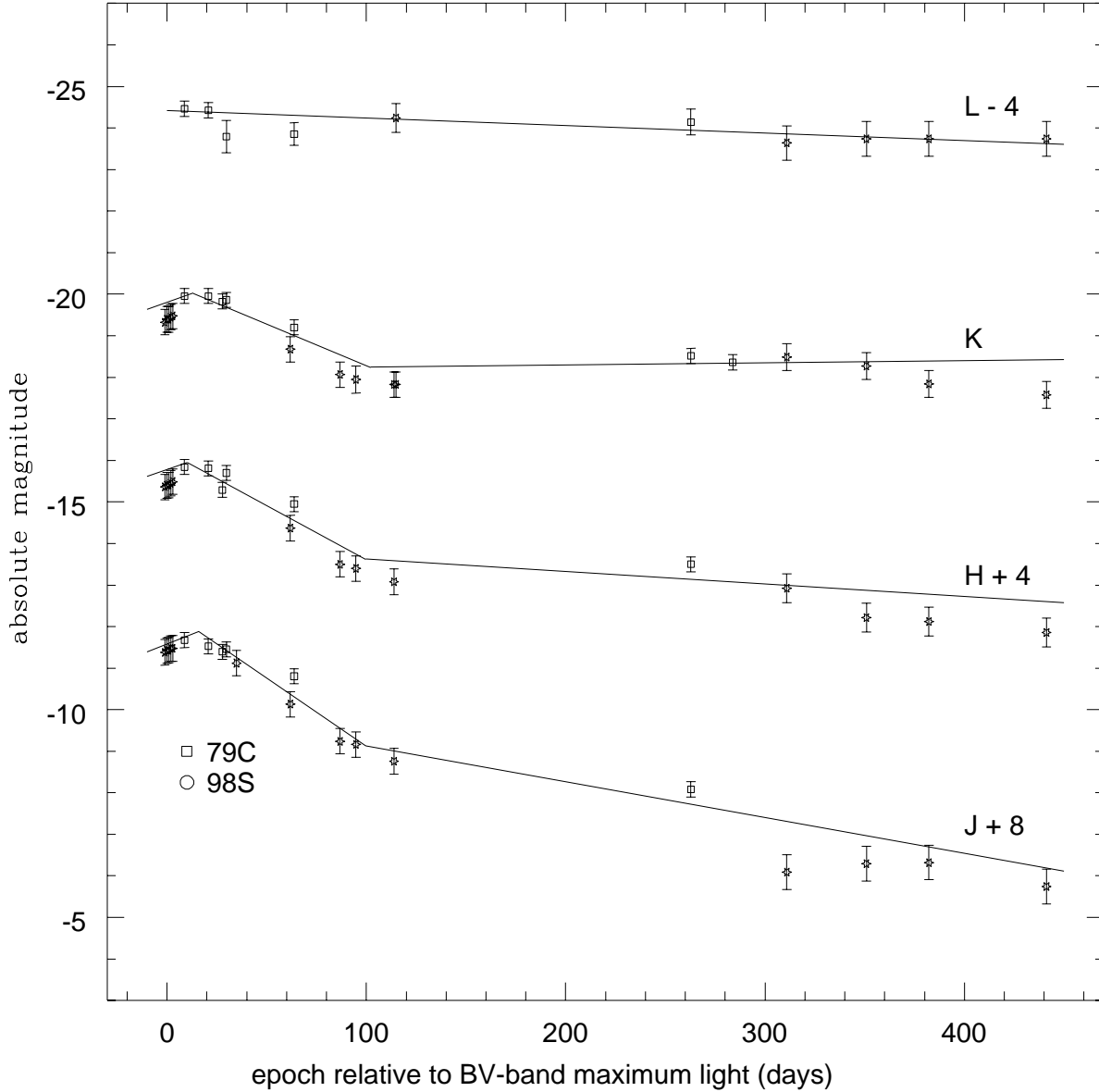
Figure 2. $JHKL$-band light curves and templates for "slowly-declining" core-collapse SNe. For clarity, the J, H, and L-band data and templates have been vertically displaced by +8, +4, and –4 magnitudes respectively. The horizontal positions of the individual light curves were set such that 0 days corresponds to BV-maximum (see text) in each case. The error bars give the combined uncertainties in photometry, extinction and distance.

We constructed absolute magnitude template light curves for the two classes. This was done as follows. Inspection of the ordinary individual JHK light curves suggested that two-component linear templates might provide a reasonable description of the data. We therefore fitted functions of this form to the entire ordinary absolute magnitude dataset in each band. Epoch +5 days was selected by visual inspection as a plausible intersection point for the two components. The template fit for the data after +5 days was then obtained in two stages. In the first step, the best-fitting

slope was determined by iteratively adjusting the vertical position of the individual SN light curves. The reason we followed this procedure was to minimise bias in the slope which would otherwise be introduced by differences in temporal coverage for different SN events having different peak magnitudes. As we were only interested in the slopes at this stage, only the photometric errors were included in the fits. Reduced χ^2 values of 20, 10, 6 were obtained in JHK respectively. The larger-than-unity values of the reduced χ^2s obtained indicates some intrinsic variations in light curve

Table 5. Template light curve of ordinary SNe

	J	H	K	L
δ_1	−0.022	−0.024	−0.021	–
M(5)	−18.39	−18.58	−18.62	−18.97
δ_2	0.027	0.026	0.022	0.013
σ_y	0.86	0.71	0.82	0.41

Table 6. Template light curve of slowly declining SNe

	J	H	K	L
δ_1	-0.019	-0.017	-0.017	0.0018
M(1)	−19.88	−19.95	−20.02	−20.42
t_1	16	10	13	0
δ_2	0.033	0.026	0.020	0.0018
M(2)	−17.12	−17.63	−18.24	-
t_2	100	100	102	-
δ_3	0.0086	0.0030	-0.00053	0.0018
σ_y	0.42	0.27	0.46	0.96

shapes between SN events. In the second step, the absolute peak magnitudes for the templates were obtained. For each band, the post-day +5 template slope was fixed at the value obtained in the procedure just described. The templates were then compared with the original, unshifted data points of individual supernovae. The vertical position of the post-day +5 lightcurve of each individual supernova was adjusted to obtain the best fit to the points *i.e.* the only free parameter was the absolute magnitude position of the lightcurve. The absolute peak magnitude of the template was then determined by taking a weighted average of the individual supernova peak magnitudes (Table 4, cols. 11-14). The weights for the events were obtained by combining the error in the apparent peak magnitude obtained in the fit with the errors in the distance modulus (±0.2–0.3 mag) and in the extinction corresponding to uncertainties in A_V of ±0.1–0.5 (see Table 4). Turning now to the pre-+5 day template component, the +5 day magnitude of this component was set to match that of the post-+5 day component. The slope of the pre-+5 day component was then varied to provide the best fit. The fits were carried out after shifting the data points vertically so that the peak magnitudes of the individual events and the template were the same. Only the photometric errors were included in the fit. Reduced χ^2s of 50, 86, and 63 in JHK respectively were obtained, indicating a considerable variation in the pre-maximum lightcurve slopes. For the L data, a single linear fit provided an adequate description. As with the JHK bands, the best slope was found by iteratively adjusting the vertical position of the individual SN light curves. This yielded a reduced χ^2 of 1.0. Again, the vertical position of the template was determined by a weighted average of the absolute magnitudes of the individual events obtained in the same way as before.

The $JHKL$ ordinary template parameters are given in Table 5. In a given band, M(5) is the absolute magnitude of the template peak at +5 days. δ_1 and δ_2 are the light curve slopes before and after epoch +5 days. The decline rates

ranged from 0.027 mags/day in J to 0.013 mags/day in L. In the bottom row we give the weighted dispersion, σ_y, of the individual supernova peak magnitudes about the peak of the template. The ordinary templates and individual data points are shown in Figure 1, where the horizontal position (epoch) is with respect to the epoch of BV-maximum = 0 days (see footnote). The error bars on the data points are the combined errors in photometry, extinction, and distance.

For the two slowly-declining SNe, we adopted three-component linear templates in JHK, with a single-component linear template in L. Guided by visual inspection, we divided the data into three eras corresponding to pre-+10 days, +10–+100 days, and post +100 days. Linear fits were then carried out for each component. Only the errors in photometry were included. The best fitting slope for the epoch between 10 and 100 days was obtained again by iteratively adjusting the vertical positions of the individual events. This slope was then used for estimating the absolute peak magnitudes of both events, and thus the vertical position of the template as before. The data points of the individual events were then shifted vertically so that their peak magnitudes matched the one of the template. This allowed us to perform linear fits for the pre-+10 day, and post-+100 day components. The magnitudes of the points of intersection (*i.e.* the template peak and inflection point) were derived from the fits. Reduced χ^2s were 41, 29, and 2 for +10–+100 days and 15, 11, and 14 for post-+100 days in JHK respectively. The value for the single-component L-band fit was 2. For the pre-+10 days, the reduced χ^2s were 4, 10, and 5 in JHK respectively. The template parameters are shown in Table 6. M(1) and t_1 give, respectively, the absolute magnitude and epoch of the template peak, while M(2) and t_2 give the absolute magnitude and epoch of the inflection. δ_1, δ_2 and δ_3 give the respective slopes for the three eras. The bottom row gives the dispersion, σ_y, of the post-+10 day points about the template. The templates and individual data points (with the photometry errors) are shown in Figure 2 where, as before, the horizontal position (epoch) is with respect to the epoch of BV-maximum = 0 days (see footnote). As already indicated, we find that up to about day +100, the decline rates are the same for both classes, to within the errors. However, the defining characteristic of the slow-decliners is the slope after +100 days. For this era, we obtain slopes of 0.0086, 0.0030, ∼0, and 0.0018 mags/day in the J, H, K, and L-band respectively. However, our study has revealed an important additional characteristic of the slow-decliners *viz.* that they are significantly more luminous than the ordinary class, even at early times. Around maximum light SNe in this class are ∼1.5 mags brighter in $JHKL$. However, it should be remembered that we have identified only 2 slow-decliners in our sample. Presumably, the slowly-declining late-time light curve of this class, and perhaps also the greater early-time luminosity, is being powered by conversion of the SN kinetic energy into IR radiation through shock interaction with the circumstellar medium and heating of dust local to the supernova (see *e.g.* Fassia *et al.* 2000a, Fassia *et al.* 2000b).

Because of the reduced extinction, and the slower light curve decline rates compared with the J- and H-bands, the K- and L-bands are superior for the purpose of a nuclear SN search. Below we examine the feasibility of detecting such

SNe using repeated K-band imaging of a sample of nearby starburst galaxies.

5   A TECHNIQUE FOR SUPERNOVA DETECTION

Having estimated the intrinsic rate of core-collapse supernova explosions (Sect. 2), determined the typical range of extinctions towards SNe in starburst galaxies (Sect. 3), and established the magnitude and shape of K-band SN light curves (Sect. 4) the next stage is to examine the efficiency with which we might detect SNe in galaxy nuclear regions.

5.1 K-band imaging of NGC 5962

We used an image pair of the IR-luminous galaxy NGC 5962 to study the efficiency of SN detection in the galaxy nuclear regions. NGC 5952 is a star-forming galaxy at a distance of 34 Mpc (Tully 1988) with a far-IR luminosity similar to the prototypical starburst galaxy M 82 ($L_{FIR} = 3.8 \times 10^{10}$ L$_\odot$).

State-of-the-art K-band images of NGC 5962 were obtained by A. Fassia, M. Hernandez and T. Geballe using UFTI (0.091"/pixel) at UKIRT[††]. Repeat images were obtained on 1999 April 4 and 5. The seeing on the first night was about 0.6" and about 1.0" on the second night. Each image comprised a mosaic pattern of 5 individual frames with 10" or 11" offsets. The total integration time for a complete image was 400–600 sec. For each of the observations a sky flat was observed with an equal exposure time and dither pattern. In addition a 5×60 sec exposure sky flat was obtained at the beginning of both nights. During the data reduction it was found that the best result for the April 4 image was achieved by using the contemporary sky flat for flat fielding. For the April 5 image, a better result was achieved with the sky flat taken at the start of the night. The images were calibrated using the UKIRT faint standards FS21 and FS25. The images are shown in Figure 3.

5.2   Supernova detection

Supernovae occurring in the nuclear regions of galaxies can be sought by comparing two images taken at different times. A rough comparison can be made by examining the images by eye and varying the contrast levels. A more efficient approach is by "blinking" the two frames. It is likely that the most sensitive search procedure is to carry out computerised subtraction of one image from the other to reveal very small differences. This is the method used in the feasibility study described here. However, for this to be practical it is necessary to first correct for the effects of differing atmospheric conditions (seeing and transparency), exposure times, focus positions and telescope guiding accuracy between the two images. Ideally, the images should all be taken with the same instrument.

5.2.1   Image Matching

Before attempting to subtract one image from another, they must first be aligned accurately. The shifts in x and y are obtainable from the positions of the galactic nucleus and any bright point sources within the images. Due to the small pixel size of UFTI, the alignment did not need to be performed to a precision of better than 1 pixel.

A more difficult problem is image mismatch owing to differences in seeing and photometric conditions between the two observations. Initially, we attempted to deal with this by matching the point spread functions (PSFs) and the intensity levels of the two images using the standard IRAF [‡‡] image matching package IMMATCH. However, this was found to give unsatisfactory results in regions around bright stars and galactic nuclei. We therefore turned to the more sophisticated Optimal Image Subtraction method of Alard & Lupton (1998) which they developed for analysis of microlensing survey images. It derives an optimal kernel solution from least squares analysis of the data. The method has the advantage that it does not require any bright isolated stars to determine the kernel but can be used on any portion of an image with high enough signal-to-noise ratio. In our feasibility study we used a new version of the method (Alard 2000) which was developed to process non-crowded field images. In this version, instead of using all the image pixels, only the regions around selected bright, but not necessarily stellar, objects are used to find the kernel since in a non-crowded image most of the pixels do not include any useful information for deriving the kernel solution. Among the bright objects we must include the innermost region of the galactic nucleus if we are to obtain a satisfactory subtraction result for the nuclear regions. Unfortunately, this makes the detection of supernovae falling on those innermost pixels impossible. In the images of NGC 5962 the size of the nuclear region involved in the kernel solution was 16 $\times$ 16 pixels making detection of SNe falling within the innermost $\sim$0.7" impossible. However, we estimate that only $\sim$20% of the supernovae would occur within this region (see Section 6). Both the nucleus and also regions around four brightest point sources ($m_K > 16$) outside the galaxy's circumnuclear regions were used for the fit. In order to get the best results, all the regions used for the fit must be within the common portion of the mosaic image. Here, all the regions used for the fitting procedure were within 30" of the nucleus and are thus easily fitted within a single field of view of a typical infrared imager.

5.2.2   Testing the Optimal Image Subtraction Method for SN detection

We used the IRAF package MKOBJECTS to add artificial SNe to the galaxy images. To set the intensity profile of the artificial SNe, an elliptical Moffat profile with a similar position angle, ellipticity and beta parameter to the real stars in the image

---

[††] The United Kingdom Infrared Telescope is operated by the Joint Astronomy Centre on behalf of the U.K. Particle Physics and Astronomy Research Council.

[‡‡] IRAF is distributed by the National Optical Astronomy Observatories, which are operated by the Association of Universities for Research in Astronomy, Inc. under contract with the National Science Foundation.
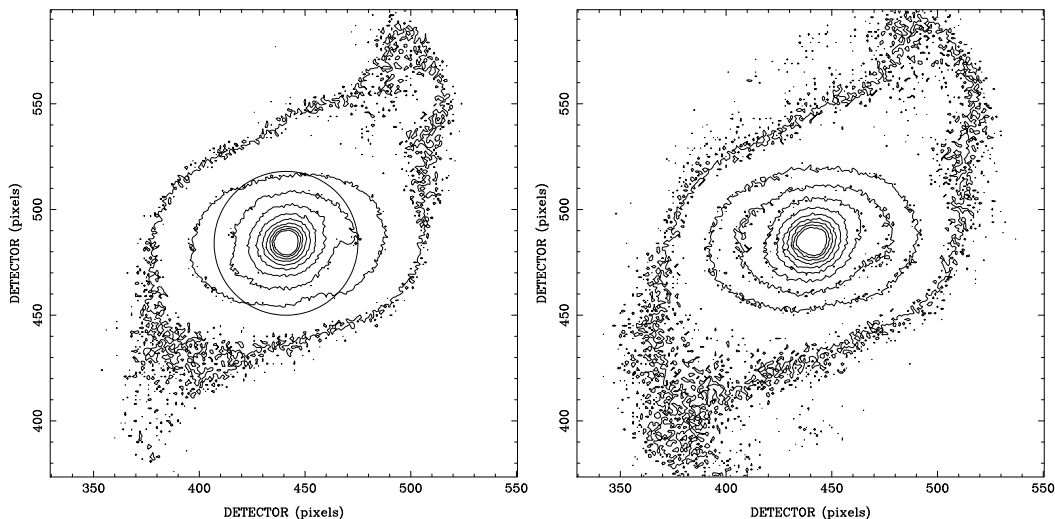
Figure 3. K-band images of NGC 5962 obtained with the UFTI camera at UKIRT (North is up and East to the left). The plate scale is 0.091" per pixel. The April 4 image (seeing FWHM=0.6") is on the left and the April 5 image (seeing FWHM=1.0") is on the right. The circle in the left hand image is of radius 500 pc ($\sim$3"). The contour interval is 40 counts. The lowest and highest contours are 50 and 410 counts which correspond to +15.9 and +13.6 mags per square arcsec, respectively, in the left hand image, and +15.7 and +13.5 mags per square arcsec, respectively, in the right hand image.
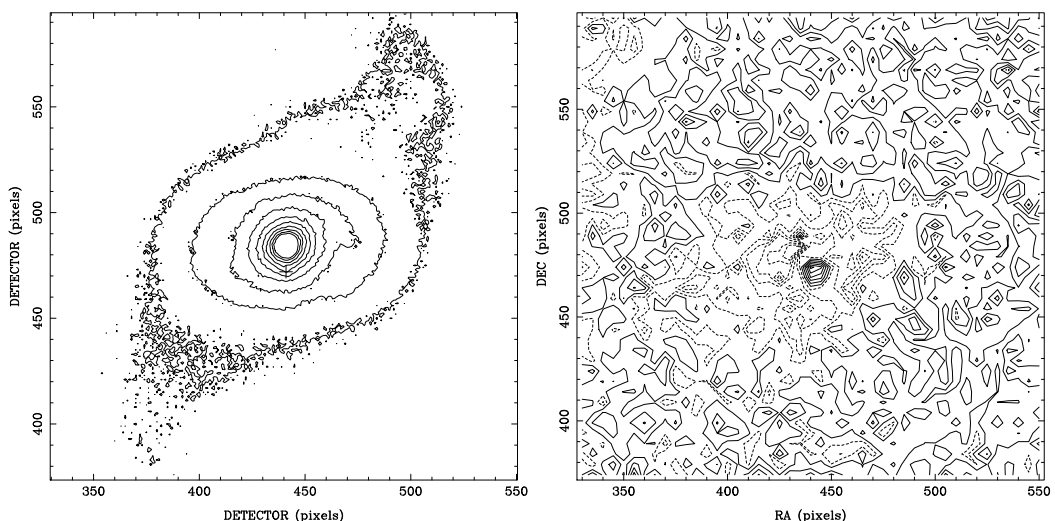

Figure 4. K-band image of NGC 5962 (seeing FWHM=0.6") with a simulated SN (cross) of m_K=17 at (441,472) (left) and after image subtraction (right). The plate scale is 0.091" per pixel. The contour interval in the subtracted image is 1 count, and the zero contour is at 2 counts, corresponding to +19.3 mags per square arcsec. The residual image (right) has been binned by $\times$5 in the x and y directions.

was used. This was set to correspond to the better-seeing image ($\sim$0.6") and the artificial supernovae were added to this image. However, since the better-seeing image is convolved to match the poorer-seeing image before the image subtraction, the size of the supernova seeing disk in the residual image is $\sim$1". An example of supernova detection is presented in Figure 4. In Figure 4(left) an artificial supernova of $m_K = +17.0$ has been placed 1.1" (180 pc) south of the centre of NGC 5962 in the better-seeing image, indicated by the cross. In the residual image (Figure 4(right)) the supernova is clearly visible.

The occurrence of 18000 supernovae was simulated, distributed randomly within the innermost 500pc radius of NGC 5962. For each simulation, subtraction was performed using the procedures described above. The residual images were then sought for point sources using the `IRAF DAOPHOT` package. The detection threshold was set at 5 times the back-

ground noise. The supernova detection efficiency at different distances from the centre of NGC 5962 is presented in Figure 5 for a range of apparent magnitudes. It shows the probability of detecting SNe of different apparent magnitudes and positions. Only in the 0-100 pc region could no supernovae be detected by this method.

6   FEASIBILITY OF SEARCHING FOR SUPERNOVAE IN THE NUCLEAR STARBURST REGIONS OF GALAXIES

The SN detection efficiency derived above is used here to determine the number of nuclear supernovae which would be discovered in a practical survey.
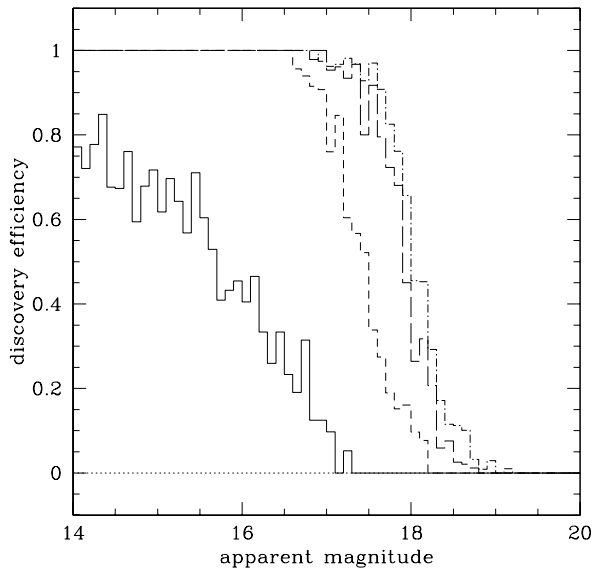
Figure 5. The fraction of simulated SNe recovered within different annulae in the K-image of NGC 5962 as a function of the SN apparent magnitude. The dotted, solid, short dashed, long dashed, and dashed-dotted lines correspond to the 0-100, 100-200, 200-300, 300-400, and 400-500pc annulae respectively.

6.1 Monte Carlo Simulations of the appearance of Supernovae

We examined the detectability of supernovae in the nuclear regions of starburst galaxies as follows. We simulated the range of absolute peak magnitudes by applying Gaussian distributions to the two types of template light curve. Average peak magnitudes of $K = -18.6$ and $K = -20.0$, and dispersions of $\sigma_K = 0.8$ and $\sigma_K = 0.5$ were adopted for the ordinary and slowly-declining SNe respectively. Since 1987, the fraction of core-collapse supernovae exploding as type IIn events listed in the Asiago Supernova Catalogue (Barbon *et al.* 1999) is 14%. However, the intrinsic rate of type IIn SNe may be smaller since their higher intrinsic brightness compared to the "ordinary" SNe means that they are more likely to be discovered. According to Cappellaro *et al.* (1997) they constitute only 2–5% of all type II SNe. However, as the proportion of slow-decliners in the nuclear starburst regions is uncertain we carried out the simulation for slow-decliner fractions ranging between 0 and 60%. The epoch of observation was allowed to vary randomly between –20 and +340 days relative to the K maximum light. The absolute magnitude for each of the events was then assigned according to the template light curves (Section 4).

The absolute magnitudes were then scaled by the appropriate extinctions and distance moduli. To simulate the effects of extinction, we carried out the study for three fixed extinction values *viz.* $A_K = 2, 3, 4$ ($A_V = 18, 27, 36$). We also carried out the simulation for a specific distribution of extinction values towards the nuclear SNe, by adopting the extinction distribution towards the SNRs in M 82. This was done by selecting an extinction for each simulated event randomly from the extinctions listed in Table 3, col. 6. In the case of the extinction lower limits the SN was assumed to be totally obscured in the K-band regardless of its magnitude, whereas the extinction upper limits listed in Table 3 (lower section) were considered as actual extinction values.

We simulated the occurrence of supernovae in galax-ies at distances of 20, 30 and 40 Mpc, and also carried out the simulation for a specific distribution of distances according to the galaxy sample described in Appendix A. This was done by selecting the distances for the simulated events from a random distribution in which each of the distances had a weight according to the corresponding galaxy's far-IR luminosity *i.e.* its SN rate. As the distance increases, not only does the supernova become fainter but also, for conservatively poor seeing of 1", the ability to spatially resolve any SN against the nuclear region rapidly diminishes. 1" at 50 Mpc corresponds to 240 pc, which is already half of our search radius. Therefore, we considered the detection of SNe within 45 Mpc only. In considering different host galaxy distances, we only varied the SN magnitudes. The actual NGC 5962 images were unchanged. For galaxies at distances less than 34 Mpc (the distance to NGC 5962) this is clearly a conservative approach because of the larger linear size of the galaxy nuclear profile compared to the size of the seeing disk. However, for galaxies more distant than NGC 5962 the reverse is true. The linear region over which the SN can be spatially resolved against the nucleus diminishes. The poorer seeing image of the NGC 5962 pair was 1.0". Thus, to achieve comparable resolution for a galaxy at 45 Mpc, we would need the seeing of the poorer image to be 0.75". We therefore assumed that in the survey, the best seeing nights would be devoted to the most distant galaxies of the sample.

The intrinsic rate of core-collapse SNe in the nuclear regions of the sample galaxies was scaled according to the galaxy FIR luminosities, L_{FIR} (see Appendix A). For the relation between the core-collapse SN rate and L_{FIR} we adopted the average of that found in NGC 253, M 82, and NGC 4038/39 *viz.* $r_{SN} / L_{FIR} = 2.7 \times 10^{-12} / L_{\odot} \ yr^{-1}$. The supernova location was based on the observation by several authors that the K-band continuum in a starburst system (*e.g.* NGC 253, Engelbracht *et al.* (1998)) is dominated by red supergiants (the progenitors of core-collapse SNe). We
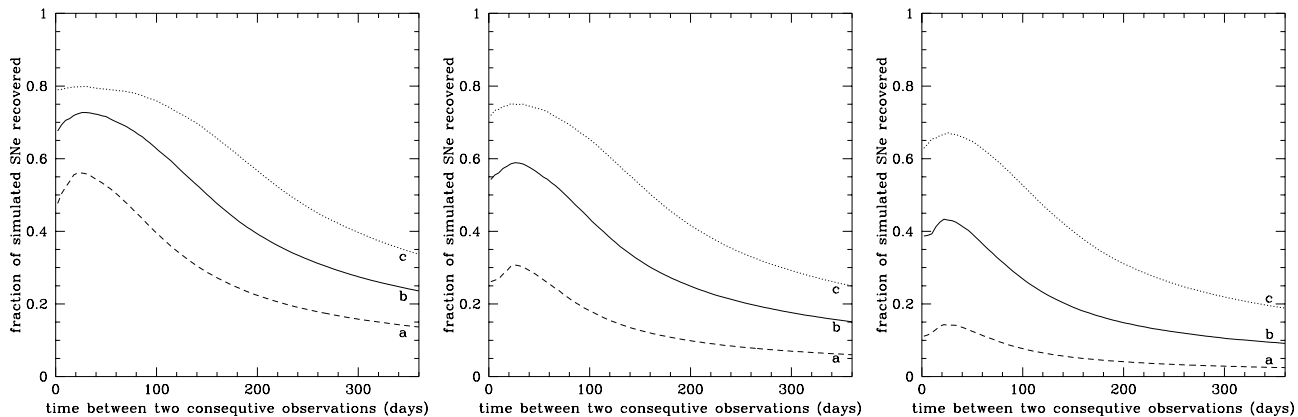
Figure 6. The fraction of simulated SNe recovered within the innermost 500 pc in the K-image of NGC 5962 for different time intervals between observations. Figures (left), (middle) and (right) correspond to simulated galaxy distances of $d = 20$, 30 & 40 Mpc respectively. In each figure, the (a) dashed, (b) solid and (c) dotted lines correspond to $A_V = 18$, 27 & 36 respectively.
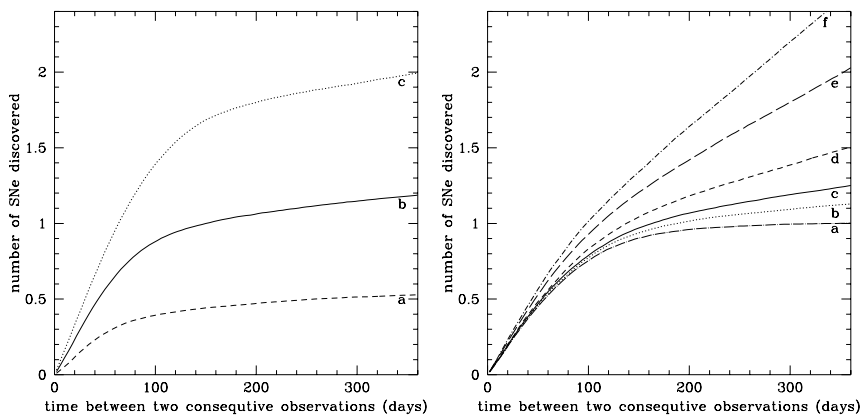

Figure 7. The total number of supernovae discoverable in a single observation of the whole galaxy sample (Table A1) as a function of the length of time since the previous observation, t_{intv}. In the LH plot, the (a) dashed, (b) solid and (c) dotted lines correspond to $A_V = 36$, 27 & 18 respectively, with a 5% fraction of slow-decliners. In the RH plot, we have adopted an M 82-like extinction distribution, and the lines a, b, c, d, e, f correspond to different intrinsic fractions of slowly-declining events viz. 0, 0.05, 0.10, 0.20, 0.40, and 0.60 respectively (see Section 6.2).

assume that this is roughly appropriate for NGC 5962 which has an $L_{\rm FIR}$ higher than NGC 253, and is classified as a "nuclear HII-region galaxy" (Misselt et al. 1999) indicating a moderate level of nuclear star formation. We therefore used the nuclear K-band light profile as being roughly representative of the SN spatial distribution. Random distributions of (x, y) coordinates were generated for the artificial supernovae, weighted according to the observed K-band light distribution of NGC 5962 within 500 pc of the centre.

6.2 Simulation of a Supernova Search

We used the simulated occurrence of the supernovae together with the supernova detection efficiency estimated above to predict the number of supernovae discoverable during an observing programme using a ∼3m telescope (e.g. the NASA Infrared Telescope Facility or the Nordic Optical Telescope). We considered a sample of 45 galaxies (see Table A1) observable in the northern hemisphere. These 45

galaxies were selected according to their far-IR luminosities, far-IR colours and distances (see Appendix A).

In Figure 6 we show, for a fixed integration time per galaxy, the fraction of simulated SNe detected in a single observation as a function of time interval, t_{intv}, since the previous observation. Each curve is based on the simulation of 100 000 SNe within the innermost 500 pc radius of NGC 5962 (see Fig. 3 left) as described in subsection 6.1. The effects of intrinsic dispersion in the supernova magnitudes and a 5% intrinsic fraction of slow-decliners have been included. Results for a range of extinctions and distances are illustrated. For example, at 30 Mpc, for a time interval of 200 days between successive observations, we find that if A_V is increased from 18 to 36 the fraction of SNe recovered is reduced by a factor of ∼4. Likewise, for an extinction of $A_V = 27$, increasing the simulated distance to the host galaxy from 20 Mpc to 40 Mpc cuts the fraction detected by a factor of ∼2.5. These results are now used along with the predicted intrinsic SN rate (*cf.* Section 2) to examine how the number

of discoverable SNe in a galaxy sample is affected by choice of t_{intv}.

In Figure 7 we show the number of supernovae discoverable from the sample of 45 galaxies for a given observation of the entire galaxy sample (assuming that the galaxy comparison images have been already acquired) as a function of the time interval, t_{intv}, since the previous observation. Again, each curve is based on the simulation of 100 000 SNe. These figures are used below to estimate the best observing strategy. The number of SNe discoverable is plotted in Fig 7 (left) for three different extinction values assuming a 5% fraction of slow-decliners, and in Fig 7 (right) for the M 82-like extinction distribution (see Table 6, col. 6). In Fig 7 (right) we also illustrate the effect of the expected higher rate of the slowly-declining events in the nuclear starburst environment. Such an enhanced rate could be due to the higher densities caused by greater stellar mass-loss, stellar winds and other, nearby SNRs in the nuclear regions (e.g. Cid Fernandes 1997). A recent study of the SNR flux variation in M 82 by Kronberg *et al.* (2000) gives indirect evidence of enhanced circumstellar densities. They found that only $\sim$25% of the sources varied measurably during a 11.8 year period, with the remaining $\sim$75% having exceptionally stable integrated flux densities. We conclude that, for $t_{intv} \sim 6$ months, if about 40% of the nuclear SNe were slowly-declining, we would expect a $\sim 35\%$ higher discovery rate than would be achieved for a $\sim$5% SNe IIn fraction.

With limiting magnitudes similar to those of the NGC 5962 images used in this feasibility study, the 45 sample galaxies (and sky flats) could be observed in $\sim$20 hours with a 3–4m telescope (K-band). In a single observation of the sample, the expected number of supernova discoveries is 1.8, 1.0, 0.5, for extinctions of $A_V = 18$, 27 and 36 respectively. This result corresponds to a time interval exceeding $\sim$6 months since the previous observation of the sample (see Figure 7(left)). If we assume that the distribution of extinctions towards the SNe is similar to that of M 82, we obtain lower and upper limits of 1.0 and 1.3 respectively for the expected number of SN detections, given slow-decliner percentage fractions of 5% and 40% respectively (see Figure 7(right)).

The adoption of the extinction distribution based on M 82, which is an edge-on galaxy, our conservative approach to simulating supernovae in galaxies closer than 34 Mpc (see Section 6), and the likely higher fraction of the slowly-declining events in the nuclear starbursts, taken together suggest that our supernova discovery rate estimates are probably lower limits.

However, even if no supernovae were discovered in an observing programme, useful upper limits could be derived for the nuclear supernova rate, assuming particular extinction values. For example, in a negative search consisting of 3, 4, or 5 observations of the sample, an upper limit for the supernova rate would be 3.1, 2.1, or 1.6 FIRSRU at 90% confidence, assuming an M 82-like extinction (Section 3), and a slow-decliner percentage fraction of 5%. Alternatively lower limits could be derived for the average extinction towards the nuclear supernovae, assuming our estimated intrinsic nuclear supernova rate of 2.7 FIRSRU. For negative surveys comprising 3, 4, and 6 observations of the sample, the extinction lower limits would be $A_K = 2$, 3, and 4 respectively, with at least 90% confidence

6.3   Observing Strategy

Given a fixed amount of telescope time, what distribution of the time will maximise the number of detected supernovae? Clearly, as we increase the integration time per galaxy we shall a) increase the volume of space within which SNe can be detected, and b) increase the amount of time after explosion during which we can detect a given SN. However, is it better to apply the same integration time to all galaxies, or to increase the integration time as we go to more distant galaxies? Keeping the integration time the same means that we can detect the much rarer nearby SNe at much later points on their light curves and so reduce the chance of missing these particularly interesting events. The disadvantage is that this procedure will sometimes "waste" time detecting a nearby SN while it is still at an early point on its light curve and therefore very bright. On the other hand, if we adjust the integration time to give a detection threshold which is at the same epoch on the light curve regardless of the galaxy distance then we can save time on the nearer events and use the time saved to increase the volume of space explored. The disadvantage is that we are more likely to miss the fewer nearby events. It can be shown that the latter strategy will yield a somewhat higher supernova detection rate. However, this ignores the fact that as we go to greater distances, the supernovae become increasingly difficult to resolve against the host galaxy nucleus. When we take that into account, the benefit of varying the integration time with distance diminishes. This fact, together with the desire to avoid missing nearby SNe suggests that working with a fixed integration time per galaxy is a reasonable strategy.

Turning now to the question of the number of times we should observe a given galaxy. For a given amount of telescope time and a fixed, uniform integration time (*i.e.* magnitude threshold) per galaxy, if we double the number of observations it simply halves the number of galaxies we can observe. In another approach which would allow a doubling of the number of times a given galaxy was observed, we could maintain the number of galaxies observed but reduce the integration time on each by a factor of two (ignoring overheads). This would effectively reduce the number of distant SNe that would be detected. The volume of space accessible above the threshold would be reduced by $2^{0.75} = 1.68$ while doubling the number of observations. This would yield a modest net gain in the detection rate of $\times 2/1.68 = \times 1.2$. So, given the overheads, there would be nothing gained in going for a larger number of shorter observations. Thus, it appears that there would be little to be gained in dividing up the telescope time into more than a few observations per galaxy.

Another issue concerns the interval between successive observations of a given galaxy, t_{intv}. Inspection of Figure 7 reveals that, at first, the SN detection rate increases quite rapidly with t_{intv}. This is due to the fact that, as t_{intv} is increased more supernovae will occur in the interval and yet we are still able to detect many of those SNe which exploded soon after the previous observation. If we work with a fixed detection threshold, then the nearer, but rarer, SNe can be detected at much later points on their light curves. As a rule of thumb, therefore, we should set t_{intv} to equal the light curve duration over which we can detect the nearest events. Less time than this will reduce the number of the nearest

events we can detect. More time than this does not increase the number of detectable "ordinary" events, but simply increases the duration of the programme. It is true that as we continue to increase t_{intv}, more slow-decliners will be found (see Figure 7(right)). However, the conservative assumption is that these form a small minority of the sample. For an "ordinary" template K-band light curve with M_K peak at –18.6 and assuming $A_K = 3$, our UFTI images suggest that the nearest likely supernova ($d{\sim}10$ Mpc) could be detected out to ${\sim}140$ days post-explosion in an integration time of 5–15 minutes on a 3–4 m telescope. Thus we are looking at t_{intv} values of at least a few months. Taking into account also the slow-decliners we conclude that telescope time is used most efficiently if the time intervals between the observations of a given galaxy are *at least* ${\sim}6$ months.

7 CONCLUSION

The feasibility of detecting supernovae in the nuclear regions of nearby starburst galaxies has been investigated. This has entailed the examination of expected SN rates, extinction, and SN magnitudes in such regions. An intrinsic SN rate of 2.7×10^{-12} $L_{\mathrm{FIR}} / L_{\odot}$ yr^{-1} was estimated. Extinction values ranging between $A_K = 2$ and 4 were judged to be typical. A particularly detailed examination of the M 82 extinction distribution was carried out. A mean A_V of 24 was obtained from hydrogen column density measurements. Template core-collapse SN light curves in $JHKL$ were assembled. Two types were identified - ordinary and slow-declining. The slow-decliners were found to be significantly more luminous than the ordinary core-collapse SNe, even at early times. Using the Optimal Image Subtraction method, it was found that supernovae outside the innermost ${\sim}1$" of a galaxy can be easily detected in K-band images. Imaging of a sample of 45 galaxies on a 6 month cycle, would probably reveal at least 1 SN per cycle. However, the actual number of detections could be significantly higher if slow-decliners are more common in nuclear regions. Near-infrared observations of SNe in nuclear starbursts will provide us with a valuable new probe of the conditions and star formation rates in the obscured starburst regions of galaxies.

REFERENCES

Alard C. & Lupton R.H., 1998, ApJ, 503, 325
Alard C., 2000, A&AS, 144, 363
Allen M.L. & Kronberg P.P., 1998, ApJ, 502, 218
Barbon R., Buondí V., Cappellaro E., Turatto M., 1999, A&AS, 139, 531
Bohlin R.C., Savage B.D., Drake J.F., 1978, ApJ, 224, 132
Bregman J.D., Temi P., Rank D., 2000, A&A, 355, 525
Buat V. & Xu C. 1996, A&A, 306, 61
Buta R.J., 1982, PASP, 94, 578
Calamai G., Govazzi G., Randone I., Tofani G., 1993, IAUCIRC, 5741, 1
Cappellaro E., Turatto M., Tsvetkov D.Y., Batrunov O.S., Pollas C., Evans R., Hamuy M., 1997, A&A, 322, 431
Cappellaro E., Evans R., Turatto M., 1999, A&A, 351, 459
Cid Fernandes R., 1997, RMxAC, 6, 201
Colina L. & Perez-Olea D., 1992, MNRAS, 259, 709
Condon J.J, 1992, ARA&A, 30, 575
Crutcher R.M., Rogstad D.H., Chu K., 1978, ApJ, 225, 784
Dahlén, T. & Fransson, C., 1999, A&A, 350, 349
de Vaucouleurs G., 1978, ApJ, 224, 710
Dwek E. *et al.*, 1983, ApJ, 274, 168
Eastman R.G., Schmidt, B.P., Kirshner R., 1996, ApJ, 466, 911
Efstathiou A., Rowan-Robinson M., Siebenmorgen R., 2000, MNRAS, 313, 734
Elias J.H., Matthews K., Neugebauer G., Persson S.E., 1985, ApJ, 296, 379
Engelbracht C.W., Rieke M.J., Rieke G.H., Kelly D.M., Achtermann J.M., 1998, ApJ, 505, 639
Evans, R.O. & Hazelbrook, H.S.W., 1985, IAUCIRC, 4119, 2
Fassia A., Meikle W.P.S, Vacca W.D., Kemp S.N., 2000a, MNRAS in press (astro-ph/0006080)
Fassia A. *et al.*, 2000b, MNRAS in press (astro-ph/0011340)
Feast, M., Pont, F., Whitelock, P., 1998, MNRAS, 298, L43
Ferrarese L. *et al.*, 1996, ApJ, 464, 568
Fesen R.A. *et al.*, 1999, AJ, 117, 725
Freedman W.L. *et al.*, 1994, ApJ, 427, 628
Genzel R. *et al.*, 1998, ApJ, 498, 579
Gerardy, C.L., Fesen, R.A., Höflich, P. & Wheeler, J.C., 2000, AJ, 119, 2968
Graham J.R., 1985, Ph.D. thesis, Imperial College of Science and Technology
Greenhouse M. A. *et al.*, 1997, ApJ, 476, 105
Grossan B., Spillar E., Tripp R., Pirzkal N., Sutin B.M., Johnson P., Barnaby D., 1999, AJ, 118, 705
Huang Z.P., Thuan T.X., Chevalier R.A., Condon, J.J., Yin Q.F., 1994, ApJ, 424, 114
Iwamoto, K., Nomoto, K., Hoflich, P., Yamaoka, H., Kumagai, S., Shigeyama, T. 1994, ApJL, 437, L115
Jorgensen, H.E., Lipunov, V.M., Panchenko, I.E., Postnov, K.A. & Prokhorov, M.E., 1997, ApJ, 486, 110
Kidger, M., Mahoney, T., Selby, M., 1993, IAUCIRC, 5795, 2
Kriss, G., 1985, IAUCIRC, 4080, 1
Kronberg, P.P., Sramek, R.A., Birk, G.T., Dufton, Q.W., Clarke, T.E. & Allen, M.L., 2000, ApJ, 535, 706
Lawrence, G.F., Paulson, A., Mason, C., Butenhoff, C., Gehrz, R.D., 1993, IAUCIRC, 5844, 3
Leonard, D.C., Filippenko, A.V., Barth, A.J. & Matheson, T., 2000, ApJ, 536, 239
Lewis, J.R. *et al.*, 1994, MNRAN, 266, L27
Madau P., Della Valle M., Panagia N., 1998, MNRAS, 297, L17
Maza, J., IAUCIRC, 1982, 3684, 1
Merrill, K.M., 1980, IAUCIRC, 3444, 3

Miller D. L. & Branch, D., 1990, AJ, 100, 530

Misselt K.A., Clayton G.C., Gordon K.D., 1999, PASP, 111, 1398

Mouri H., Kawara K., Taniguchi Y., 1997, ApJ, 484, 222

Muller, A., Pizarro, O., 1982, IAUCIRC, 3739, 1

Muller, A., 1982, IAUCIRC, 3740, 1

Muxlow T.W.B., Pedlar A., Wilkinson P.N., Axon D.J., Sanders E.M., De Bruyn A.G., 1994, MNRAS, 266, 455

Neff, S.G. & Ulvestad, J.S., 2000, AJ, 120, 670

Neininger N., Guelin M., Klein U., Garcia-Burillo S. Wielebinski R. 1998, A&A, 339, 737

Odewahn S., Bailey J., 1993, IAUCIRC, 5760, 1

Panagia, N. *et al.*, 1980, MNRAS, 192, 861

Puxley P.J., Brand P.W.J.L., Moore T.J.T., Mountain C.M., Nakai N., Yamashita T. 1989, ApJ, 345, 163

Puxley P.J., Mountain C.M., Brand P.W.J.L., Moore T.J.T., Nakai, N., 1997, ApJ, 485, 143

Richmond M.W., Treffers, R.R., Filippenko, A.V., Paik, Y., Leibundgut, B., Schulman, E., 1994, AJ, 107, 1022

Richmond M.W. *et al.*, 1996, AJ, 111, 327

Richmond M.W., Filippenko A.V., Galisky J., 1998, PASP, 110, 553

Rieke G.H. & Lebofsky M.J., 1985, ApJ, 288, 618

Romanishin, W., 1993, IAUCIRC, 5773, 1

Rowan-Robinson M. & Crawford J., 1989, MNRAS, 238, 523

Rowan-Robinson M. *et al.*, 1997, MNRAS, 289, 490

Sanders D.B. & Mirabel I.F., 1996, ARA&A, 34, 749

Satyapal S. *et al.*, 1995, ApJ, 448, 611

Schlegel, D.J., Finkbeiner, D.P. & Davis, M., 1998, ApJ, 500, 525

Schmidt, M., 1968, ApJ, 151, 393

Schmidt, B.P. *et al.*, 1993, AJ, 105, 2236

Silva L., Granato G.L., Bressan A., Danese L., 1998, ApJ, 509, 103

Smith J.A., 1993, IAUCIRC, 5780, 1

Smith H.E., Lonsdale C.J., Lonsdale C.J., Diamond P.J., 1998, ApJL, 493, L17

Soifer B.T. *et al.*, 1987, ApJ, 320, 238

Soifer B.T., Boehmer L., Neugebauer G., Sanders D.B., 1989, ApJ, 98, 3

Sullivan M., Ellis R., Nugent P., Smail I., Madau P., 2000, astro-ph/0007228

Tarchi, A. *et al.*, 2000, A&A, 358, 95

Tammann G.A. & Sandage A., 1968, ApJ, 151, 825

Tammann G.A. & Schröder A., 1990, A&A, 236, 149

Terlevich R., Tenorio-Tagle G., Franco J., Melnick J., 1992, MNRAS, 255, 713

Thronson H.A. Jr. & Telesco C. M., 1986, ApJ, 311, 98

Tsujimoto, T., Yoshii, Y., Nomoto, K., Matteucci, F., Thielemann, F. & Hashimoto, M., 1997, ApJ, 483, 228

Tully R.B., 1988, Nearby galaxies catalog, Cambridge and New York, Cambridge University Press, 1988

Ulvestad J.S. & Antonucci R.R.J., 1994, ApJL, 424, L29

Ulvestad J.S. & Antonucci R.R.J., 1997, ApJ, 488, 621

Ulvestad J.S., 2000, AJ, 120, 278

Van Buren, D. & Norman, C.A., 1989, ApJL, 336, L67

Van Buren D. & Greenhouse M.A., 1994, ApJ, 431, 640

Van Buren D., Jarrett T., Terebey S., Beichman C., Shure M., Kaminski C., 1994, IAUCIRC, 5960, 2

Veron-Cetty M.-P. & Veron P., 1998, A Catalogue of quasars and active nuclei, Edition: 8th ed., Publisher: Garching: European Southern Observatory (ESO), 1998, Series: ESO Scientific Report Series vol no: 18

Wada, T. & Ueno, M., 1997, AJ, 113, 231

Weiß A., Neininger N., Hüttemeister S., Klein U., 2000, A&A in press (astro-ph/0010541)

Wills K.A., Pedlar A., Muxlow T.W.B., 1998, MNRAS, 298, 347

Yun M.S., Ho P.T.P., Lo K.Y., 1993, ApJL, 411, L17

APPENDIX A: THE GALAXY SAMPLE FOR THE DISCUSSED OBSERVING PROGRAMME

Rowan-Robinson & Crawford (1989) considered the far-IR spectra of galaxies as arising from a mixture of 1) a cool disc component, 2) a warm starburst component, and 3) a hot Seyfert component. They determined the relative proportions, α_j, of the spectrum attributable to each of the components by fitting models to the far-IR spectra of the galaxies. They plotted IRAS colour-colour diagrams for the flux density ratios: $S(25)/S(12)$ v.$S(60)/S(25)$ and $S(100)/S(60)$ v. $S(60)/S(25)$. In these plots, the starburst galaxies occupy well-defined areas and thus the far-IR flux ratios can be used as selection criteria for the galaxy sample.

We selected galaxies from Soifer *et al.* (1987, 1989) and Rowan-Robinson & Crawford (1989) whose far-IR luminosity is greater or comparable to those of M 82 and NGC 253, excluding galaxies whose far-IR luminosity is powered by a population of old stars or an AGN.
We used the following criteria for selecting the sample :

1a) for galaxies with $d \leq 25$Mpc : $L_{\rm FIR} > 1.7 \times 10^{10}$ L$_\odot$

1b) for galaxies with 25Mpc $< d \leq 35$Mpc : $L_{\rm FIR} > 2.5 \times 10^{10}$ L$_\odot$

1c) for galaxies with 35Mpc $< d \leq 45$Mpc : $L_{\rm FIR} > 3.2 \times 10^{10}$ L$_\odot$

2a) $S(25)/S(12) > 2.2$, $S(60)/S(25) < 8.1$, $S(100)/S(60) < 2.2$

2b) from Rowan-Robinson & Crawford (1989) the galaxies with $\alpha_2 > 0.6$

3) Seyfert 1 galaxies listed in Veron-Cetty and Veron (1998) were excluded.

The flux ratios, FIR luminosities $(L(8\text{-}1000\mu m)$ (Sanders & Mirabel 1996) and distances (Tully 1988) for the selected galaxies are presented in Table A1, cols. 2-6. In cols. 7-8, a lower and upper limit for the intrinsic SN rate are presented according to (a) equation (4) with $\epsilon = 1$, and (b) equation (5). In estimating the number of supernovae discoverable in an observing programme we assumed that, for most of the 45 sample galaxies, the fraction of their far-IR luminosity which is powered by young massive stars is similar to that of NGC 253 and M 82. However, for the Seyfert 2 galaxies in the sample we reduced this fraction by a factor of two, with the SN rates correspondingly reduced.

APPENDIX B: INFRARED PHOTOMETRY OF CORE-COLLAPSE SUPERNOVAE

This paper has been produced using the Royal Astronomical Society/Blackwell Science LaTeX style file.

Table A1. The galaxy sample. The flux densities are taken from Soifer *et al.* (1989) and Rowan Robinson & Crawford (1989), and the distances mostly from Tully 1988. For MGC-05-17-009, MGC-05-18-003, ESO 320-G30, ESO 402-G26, NGC 3690, UGC 3630 the distances were obtained from the recession velocities with respect to the Local Group ($H_0 = 70$ kms^{-1}/Mpc). For NGC 253 and M 82 the distances were adopted from de Vaucouleurs (1978) and Tammann & Sandage (1968) respectively, and for NGC 4038/39 the same distance was assumed as in Neff & Ulvestad (2000). The far-IR luminosities ($L(8\text{-}1000\mu m)$) were calculated from the given flux densities and distances according to Sanders & Mirabel (1996). The far-IR luminosities are converted to the intrinsic SN rates according to (a) Equ. 5 and (b) Equ. 1 in Section 2. The values given in column (a) were obtained assuming $\epsilon = 1$ and so are probably lower limits.

Galaxy	$\frac{S(25)}{S(12)}$	$\frac{S(100)}{S(60)}$	$\frac{S(60)}{S(25)}$	$\mathrm{Log}(L_{\mathrm{FIR}})$ [L$_\odot$]	d [Mpc]	$\mathrm{r}_{SN,intr}$ (a)	(b)
NGC 253	3.77	2.00	6.76	10.28	2.5	0.02	0.05
NGC 470	3.37	1.69	5.14	10.41	33	0.03	0.07
NGC 520	3.34	1.48	10.38	10.89	30	0.09	0.21
NGC 660	2.68	1.45	9.07	10.53	13	0.04	0.09
NGC 1022	4.62	1.37	5.80	10.36	20	0.03	0.06
NGC 1068	2.33	1.30	2.16	11.31	15	0.12	0.28
NGC 1222	3.78	1.18	5.77	10.61	33	0.04	0.11
NGC 1482	3.05	1.29	7.47	10.65	21	0.05	0.12
UGC 3630	3.65	1.75	7.30	10.27	23	0.02	0.05
MGC-05-17-009	3.45	1.40	6.44	10.81	39	0.07	0.17
MGC-05-18-003	3.10	1.73	7.99	10.68	39	0.05	0.13
NGC 2339	3.99	1.68	8.83	10.77	33	0.06	0.16
NGC 2799	4.0	1.42	6.84	10.73	29	0.06	0.14
NGC 2964	2.39	1.94	6.85	10.35	23	0.02	0.06
M 82	3.99	1.03	4.60	10.62	3.25	0.05	0.11
NGC 3094	3.44	1.31	3.94	10.66	34	0.05	0.12
NGC 3256	4.80	1.28	6.08	11.57	37	0.40	1.00
NGC 3310	3.24	1.40	6.46	10.62	20	0.05	0.11
NGC 3395	3.30	1.62	7.58	10.43	29	0.03	0.07
NGC 3471	3.46	1.50	7.07	10.49	35	0.03	0.08
NGC 3504	3.73	1.57	5.39	10.75	28	0.06	0.15
NGC 3597	3.32	1.28	6.63	10.87	44	0.08	0.20
NGC 3690	6.19	1.01	5.04	11.84	45	0.75	1.9
NGC 3885	3.81	1.37	6.49	10.45	30	0.03	0.08
ESO 320-G30	4.05	1.28	14.68	11.17	42	0.16	0.40
NGC 4038/39	2.66	1.69	7.40	10.83	21	0.07	0.18
NGC 4102	4.01	1.50	7.13	10.68	18	0.05	0.12
NGC 4194	5.44	1.02	5.61	11.09	42	0.14	0.31
NGC 4536	2.44	1.56	7.35	10.24	14	0.02	0.05
NGC 4691	3.72	1.50	4.65	10.44	24	0.03	0.07
NGC 5073	5.41	1.48	5.80	10.61	39	0.05	0.11
NGC 5188	3.71	1.54	7.97	10.90	35	0.09	0.21
NGC 5218	3.03	1.98	7.67	10.60	41	0.04	0.11
NGC 5430	2.95	1.99	5.64	10.82	42	0.07	0.18
NGC 5597	3.25	1.91	4.92	10.72	41	0.06	0.14
NGC 5915	2.87	1.41	7.84	10.60	36	0.04	0.11
NGC 5929	3.77	1.50	5.64	10.68	41	0.03	0.06
NGC 6000	4.02	1.61	7.35	11.04	32	0.12	0.30
NGC 6764	3.55	1.79	4.77	10.51	38	0.04	0.09
NGC 6835	3.00	1.48	7.19	10.33	25	0.02	0.06
ESO 402-G26	2.44	1.59	8.71	10.49	39	0.03	0.08
NGC 7479	2.80	1.60	3.92	10.84	35	0.04	0.09
NGC 7552	4.02	1.37	6.04	11.06	23	0.12	0.31
NGC 7582	4.69	1.50	7.48	10.73	20	0.03	0.07
NGC 7714	6.00	1.11	3.73	10.72	40	0.06	0.14

Table B1. Infrared photometry of core-collapse supernovae

Supernova	Date	J	H	K	L	Source
SN 1979C	43987.8	11.56(5)	11.32(5)	11.16(5)	10.61(7)	Merrill private communication
	43999.8	11.71(5)	11.35(5)	11.16(5)	10.65(7)	Merrill private communication
	44006.8	11.84(5)	11.87(5)	11.29(5)	-	Merrill private communication
	44008.8	11.78(5)	11.46(5)	11.25(5)	11.28(33)	Merrill private communication
	44042.8	12.43(5)	12.21(5)	11.91(6)	11.22(20)	Merrill private communication
	44241.8	15.15(7)	13.66(6)	12.60(6)	10.93(25)	Merrill private communication
	44262.8	-	-	12.75(7)	-	Merrill private communication
SN 1980K	44544.5	10.46(5)	10.23(5)	10.07(10	9.66(10)	Dwek et al. (1983)
	44545.5	10.49(5)	10.40(5)	10.18(5)	9.92(15)	Dwek et al (1983)
	44547.5	10.40(5)	10.28(5)	10.10(5)	9.88(6)	Dwek *et al.* (1983)
	44551.5	10.58(5)	10.43(5)	10.24(5)	9.97(5)	Dwek *et al.* (1983)
	44552.5	10.55(5)	10.42(5)	10.22(5)	9.89(6)	Dwek *et al.* (1983)
	44557.5	10.71(5)	10.56(5)	10.35(5)	10.05(7)	Dwek *et al.* (1983)
	44558.5	10.60(5)	10.53(5)	10.33(5)	10.00(15)	Dwek *et al.* (1983)
	44559.5	10.78(5)	10.64(5)	10.40(5)	10.14(9)	Dwek *et al.* (1983)
	44576.5	11.13(5)	10.93(5)	10.64(5)	10.35(7)	Dwek *et al.* (1983)
	44592.5	11.48(5)	11.30(5)	10.97(5)	10.55(6)	Dwek *et al.* (1983)
	44755.5	16.71(14)	16.09(19)	14.69(18)	12.60(15)	Dwek *et al.* (1983)
	44774.5	16.71(14)	16.22(13)	14.95(13)	-	Dwek *et al.* (1983)
SN 1982E	45158.5	17.39(10)	15.47(5)	13.81(3)	-	Graham (1985)
	45175.5	-	16.0(40)	14.3(15)	-	Graham (1985)
	45184.5	18.28(9)	15.96(4)	14.19(3)	-	Graham (1985)
	45225.5	-	-	14.91(6)	-	Graham (1985)
	45248.5	-	17.78(11)	15.60(5)	-	Graham (1985)
	45304.5	-	-	17.1(30)	-	Graham (1985)
SN 1982R	45269.6	14.0(10)	14.2(10)	13.9(10)	-	Muller (1982)
	45304.5	15.29(4)	15.06(4)	14.71(6)	-	Graham (1985)
	45329.5	16.04(5)	15.92(7)	15.31(6)	13.0(30)	Graham (1985)
	45330.5	15.87(5)	16.06(7)	15.34(6)	-	Graham (1985)
SN 1983I	45493.8	14.39(11)	13.93(7)	13.90(5)	-	Elias *et al.* (1985)
	45496.6	14.47(6)	13.97(4)	13.96(3)	-	Elias *et al.* (1985)
	45538.7	15.91(6)	15.15(4)	15.16(7)	-	Elias *et al.* (1985)
	45539.7	15.80(8)	15.08(5)	15.13(5)	-	Elias *et al.* (1985)
	45543.7	16.10(7)	15.22(5)	15.20(6)	-	Elias *et al.* (1985)
SN 1983N	45527.3	11.06(3)	11.17(3)	10.87(3)	-	Panagia *et al.* in preparation
	45528.3	10.96(3)	11.16(3)	10.87(5)	-	Panagia *et al.* in preparation
	45529.3	10.84(3)	10.96(2)	10.76(3)	-	Panagia *et al.* in preparation
	45531.8	-	-	10.64(3)	-	Panagia *et al.* in preparation
	45534.3	10.45(3)	10.61(3)	10.31(3)	-	Panagia *et al.* in preparation
	45538.8	10.42(3)	10.38(3)	10.36(3)	10.17(5)[a]	Panagia *et al.* in preparation
	45540.0	10.49(2)	10.32(2)	10.21(2)	10.21(20)	Panagia *et al.* in preparation
	45540.7	10.55(6)	10.37(5)	10.23(5)	10.20(20)	Panagia *et al.* in preparation
	45541.7	10.47(6)	10.32(5)	10.19(5)	10.04(13)	Panagia *et al.* in preparation
	45559.5	11.05(6)	10.76(7)	10.91(13)	-	Panagia *et al.* in preparation
	45561.5	11.11(6)	10.95(8)	10.75(12)	-	Panagia *et al.* in preparation
	45577.5	11.66(10)	11.31(14)	11.41(23)	-	Panagia *et al.* in preparation
	45738.0	-	-	14.58(8)	-	Elias *et al.* (1985)
	45807.8	-	-	15.78(14)	-	Elias *et al.* (1985)
	45829.8	-	-	16.77(44)	-	Elias *et al.* (1985)
	45862.7	-	-	17.52 (94)	-	Elias *et al.* (1985)
SN 1984L	45959.7	13.26(9)	13.07(8)	12.87(7)	-	Elias *et al.* (1985)
	45979.7	13.63(4)	13.32(4)	13.20(4)	-	Elias *et al.* (1985)
	46008.6	14.49(6)	14.00(4)	-	-	Elias *et al.* (1985)
	46009.6	14.42(4)	13.91(4)	13.97(4)	-	Elias *et al.* (1985)
	46050.6	15.62(8)	14.88(5)	15.05(4)	-	Elias *et al.* (1985)
SN 1985L	46265.5	12.62(2)	12.47(2)	12.38(3)	12.22(41)	Meikle private communication
	46292.8	12.96(5)	12.81(5)	12.70(7)	12.87(65)	Meikle private communication
	46293.8	-	-	12.75(7)	12.81(63)	Meikle private communication
	46302.5	13.21(1)	12.92(4)	12.95(4)	12.75(74)	Meikle private communication

[a] The L-band magnitudes given for SN 1983N were observed in L'-band.

Supernova	Date	J	H	K	L	Source
SN 1985P	46419.1	13.02(2)	12.88(2)	12.61(2)	-	Meikle private communication
	46477.1	15.29(13)	15.08(12)	14.70(17)	-	Meikle private communication
	46518.1	15.46(4)	15.49(9)	15.04(10)	-	Meikle private communication
	46520.1	15.90(3)	15.92(7)	15.36(13)	-	Meikle private communication
	46594.1	17.32(9)	17.74(27)	17.9(1.4)	-	Meikle private communication
SN 1990E	47938.6	14.56(20)	14.44(20)	-	-	Schmidt *et al.* (1993)
	47939.6	14.42(20)	14.26(20)	-	-	Schmidt *et al.* (1993)
	47943.6	14.14(20)	14.21(20)	-	-	Schmidt *et al.* (1993)
	47965.6	13.57(20)	13.44(20)	-	-	Schmidt *et al.* (1993)
SN 1993J	49078.4	10.57(5)	10.48(5)	10.41(5)	-	Calamai *et al.* (1993)
	49078.7	10.54(2)	10.47(2)	10.37(2)	-	Odewahn *et al.* (1993)
	49079.8	10.62(1)	10.49(1)	10.33(1)	-	Odewahn *et al.* (1993)
	49080.9	10.91(5)	10.66(5)	10.36(8)	-	Lawrence *et al.* (1993)
	49091.7	10.22(2)	10.15(2)	9.91 (2)	-	Romanishin *et al.* (1993)
	49092.7	10.18(2)	10.15(2)	9.87(2)	-	Romanishin *et al.* (1993)
	49093.6	10.13(2)	10.09(2)	9.89(2)	-	Romanishin *et al.* (1993)
	49094.6	10.10(2)	10.07(2)	9.83(2)	-	Romanishin *et al.* (1993)
	49095.6	10.05(2)	10.05(2)	9.82(2)	-	Romanishin *et al.* (1993)
	49096.6	10.04(2)	10.04(2)	9.82(2)	-	Romanishin *et al.* (1993)
	49097.7	10.02(3)	10.02(3)	9.84(3)	-	Smith *et al.* (1993)
	49098.7	10.01(5)	10.00(5)	9.80(5)	-	Lawrence *et al.* (1993)
	49098.8	10.05(3)	10.02(3)	9.85(3)	-	Smith *et al.* (1993)
	49099.7	10.05(3)	9.97(3)	9.85(3)	-	Lawrence *et al.* (1993)
	49099.7	10.06(3)	10.02(3)	9.87(3)	-	Smith *et al.* (1993)
	49101.6	10.14(3)	10.04(3)	9.89(3)	-	Smith *et al.* (1993)
	49102.7	10.16(1)	10.09(3)	9.89(3)	-	Smith *et al.* (1993)
	49103.0	10.15(6)	-	-	-	Wada & Ueno (1997)
	49104.1	10.23(16)	-	-	-	Wada & Ueno (1997)
	49105.1	9.79(38)	-	-	-	Wada & Ueno (1997)
	49107.3	-	-	10.01(4)	-	Kidger *et al.* (1993)
	49109.3	-	-	10.20(3)	-	Kidger *et al.* (1993)
	49113.3	-	10.32(4)	10.16(4)	-	Kidger *et al.* (1993)
	49114.3	10.87(4)	10.53(4)	10.35(4)	-	Kidger *et al.* (1993)
	49120.8	10.92(2)	10.48(3)	10.48(3)	-	Lawrence *et al.* (1993)
	49122.2	10.81(8)	-	-	-	Wada & Ueno (1997)
	49123.1	10.85(13)	-	-	-	Wada & Ueno (1997)
	49124.2	10.88(6)	-	-	-	Wada & Ueno (1997)
	49129.1	10.98(4)	-	-	-	Wada & Ueno (1997)
	43134.0	11.11(9)	-	-	-	Wada & Ueno (1997)
	49135.0	11.11(8)	-	-	-	Wada & Ueno (1997)
	49160.7	12.45(9)	11.69(6)	11.20(9)	-	Lawrence *et al.* (1993)
	49175.7	13.03(15)	12.13(7)	11.73(12)	-	Lawrence *et al.* (1993)
	49183.7	12.92(9)	12.51(6)	11.89(10)	-	Lawrence *et al.* (1993)
SN 1994I	49459.0	-	-	12.56(4)[a]	-	Grossan *et al.* (1999)
SN 1998S	50889.0	12.11(1)	12.06(1)	12.05(2)	-	Fassia *et al.* (2000)
	50890.0	12.07(1)	12.02(1)	11.98(2)	-	Fassia *et al.* (2000)
	50890.9	12.06(1)	12.01(1)	11.98(2)	-	Fassia *et al.* (2000)
	50891.9	12.02(1)	11.97(1)	11.93(4)	-	Fassia *et al.* (2000)
	50892.9	12.02(1)	11.93(2)	11.90(2)	-	Fassia *et al.* (2000)
	50924.9	12.37(1)	-	-	-	Fassia *et al.* (2000)
	50951.9	13.36(2)	13.05(3)	12.70(4)	-	Fassia *et al.* (2000)
	50976.8	14.25(2)	13.92(2)	13.31(5)	-	Fassia *et al.* (2000)
	50984.8	14.33(1)	14.02(2)	13.43(11)	-	Fassia *et al.* (2000)
	51003.9	14.73(6)	14.34(6)	13.55(1)	-	Fassia *et al.* (2000)
	51004.9	-	-	13.55(1)	11.1(15)	Fassia *et al.* (2000)
	51200.9	17.4(25)	14.5(15)	12.89(10)	11.7(25)	Fassia private communication
	51240.9	17.2(25)	15.2(15)	13.10(10)	11.6(25)	Fassia private communication
	51272.2	17.17(25)	15.3(15)	13.54(10)	11.6(25)	Fassia private communication
	51331.2	17.75(25)	15.56(15)	13.80(10)	11.6(25)	Fassia private communication

[a] The *K*-band magnitude given for SN 1994I was observed in *K'*-band.